TRANSACTIONS ON TRANSPORT SCIENCES

Ministry of Transport

TRANSPORT
RESEARCH
CENTRE

CZECH TECHNICAL UNIVERSITY

International Editorial Board

Causes of long-term deflections of large-span pre-stressed concrete box girders and recommendations on how to avoid these

V. Křístek[*], L. Vráblík, V. Hrdoušek
Czech Technical University in Prague, Czech Republic
* Corresponding author: vladimirkristek@seznam.cz

ABSTRACT: The results of the presented solutions and the developed analytical and design methods will help in creating the sufficient theoretical tools for the reliable and economic structural design of bridges without deflection impairments. The paper reviews the causes of under-estimation of long-term future deflections. Special attention is placed on pre-stressing - a procedure to find the optimal arrangement of tendon layout - is presented, facilitating the avoidance of tendons contributing to deflection increases. A developed computer program is freely available and a method of repair procedure and a repair example, as well as recommendations for the design practice are also presented.

KEY WORDS: bridge, creep, deflection, pre-stressed concrete, shear

1   GENERAL GUIDELINES

The design of structures is more and more directed towards the entire lifetime design with multiple concurrent objectives. Apart from durability, the most important factor in the whole life design of reinforced and, in particular, pre-stressed concrete bridges, is the Service Limit State. From this point of view, pre-stressed concrete bridges are very sensitive to a long-term increase of deflections. This phenomenon has a paramount importance for serviceability, durability and the long-time reliability of such bridges.

Due to excessive deflections, several bridges had to be either closed or repaired well before the end of their initially projected lifespan. The cost of reduced service life of structures is tremendous for society, the owners and users. In fact, it greatly exceeds, in strictly economic terms, the cost of catastrophic failure, due to a badly predicted safety margin.

Reliable prediction of bridge deflections during their construction, as well as during their service life, is of crucial importance for achieving good durability and long-term serviceability. Obviously, the difficulty of predicting deflections is closely related to the properties of concrete (strength, elastic modulus, nonlinearity, creep, shrinkage, etc.), both initially and over time.

The long-term deflection behaviour of long-span pre-stressed concrete box girder bridges has often deceived engineers monitoring the deflections. A survey of many bridges monitored in various countries showed that all of them have experienced similar deflection histories. It has frequently been experienced that the box girders of many pre-stressed concrete bridges deflected far more than predicted in design. The deflection evolution has often been counterintuitive, with slowly growing deflections in the early years, followed later by a rapid and excessive deflection growth.

Six different causes of the deflection problems may be discerned:

1   Design based on an obsolete, oversimplified and unrealistic model for predicting creep, and the shrinkage properties of concrete, or of cross sections of concrete girders (Bažant 2000, Křístek et al. 2006).

2   An obsolete and unrealistic method of time-dependent analysis of structural effects of creep and shrinkage, based, for instance, on assuming the creep and shrinkage properties to be homogeneous throughout the cross section and ignoring the effects of differences of shrinkage and drying creep between the top and bottom slabs of the box girder (Křístek et al. 2006), which result from differences in drying half-times engendered by differences principally in slab thickness and secondarily in temperature history.

3   Lack of updating of the long-time creep and shrinkage predictions by means of short-time (1 month) creep and shrinkage tests and water loss tests of the particular concrete to be used (Bažant and Baweja 2000).

4   Absence of statistical deflection predictions, ignoring the large random scatter in concrete creep and shrinkage effects, and especially the fact that the total observed deflection is the difference of two large numbers—the deflection due to external loads, and the deflection due to pre-stress (a difference of large numbers is greatly sensitive to a small change in one of these numbers and may thus result in a significant change of thedifference, i.e., in a significant change of the total deflection value).

5   Incorrect and harmful tendon layout—some tendon layouts benefiting the stress state can atthe same time be harmful from the deflection viewpoint. Therefore, bridge design should be performed on two different levels: not only the common stress analysis, but also optimization of pre-stressing tendon layout to minimize deflections.

6   An oversimplified structural model—particularly the use of the classical mechanics of beam bending, based on the Bernoulli-Navier hypothesis of cross-sections remaining plane, while the true behavior is three-dimensional, with a strong shear lag, due to large shear deformations in the webs and plates.

Let us now discuss point 5 in more detail.

2   DEFLECTION INCREASE DUE TO INCORRECT AND HARMFUL TENDON LAYOUT

The choice of pre-stress tendon layout, i.e., the location and profile, is often governed by construction stages, as well as the cross-section geometry. But it is important to optimize the layout of tendons, so as to minimize deflections. Low deflections during the cantilever construction stages do not ensure acceptable deflections during the service life. The tendons installed during cantilever erection stages are usually very efficient during construction. However, after changes of the structural system (e.g. closing of the mid-span joints) to make the structure continuous, the cantilever tendons might not significantly inhibit the long-term deflection growth because creep produces additional forces, due to the redundancy of the new structural system.

The consequences of the tendon layout for deflections have been elucidated and a method to assess them quantitatively has been developed (Křístek and Vráblík, 2007). The advantage of this method is its ease of application, which allows the optimal tendon layout to be readily determined. The method has been programmed and is freely available on a web site and is proposed as a simple design aid avoiding expensive solutions. The practicing engineers can benefit in the design of sensitive bridges from the computer program OPTI 1.1, which has been developed at the Czech Technical University in Prague to make the assessment of the tendon layout immediately accessible to any engineer. This program is free to download from the Internet address: http://concrete.fsv.cvut.cz/veda/science_en.php. It suffices to fill out the boxes for the data on the bridge and its tendon layouts, and the output

is the deflection contributions of the individual tendons. The location of a tendon that is most efficient for reducing deflections can be determined in such a way.

Let us now present an example from practice, elucidating the significance of tendon layout and the efficiency of various layouts in reducing the deflections. The example is the bridge over the river Labe (Elbe) in Mělník: A three-span tapered continuous box girder (with spans 72.05 + 146.2 + 72.05 m; Fig. 1), built in 1992 in Central Bohemia and erected using the cantilever technology. We are interested in identifying a possible unsuitable tendon layout that would be harmful, causing a long-time increase (rather than a decrease) of the mid-span deflection.
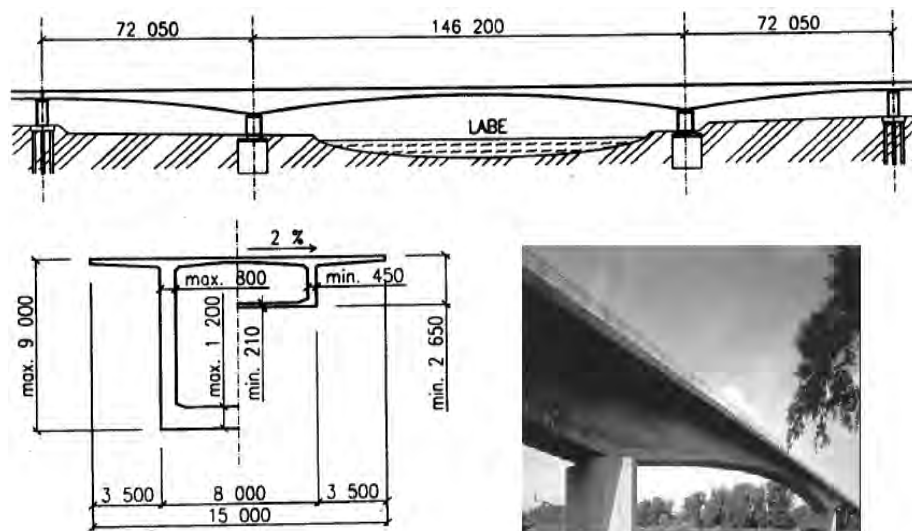
Figure 1: Bridge over the River Labe (Elbe) in Mělník.

Tendons of several categories were installed during the individual stages of the construction process (Fig. 2). The effects of individual tendons were evaluated by applying the above mentioned computer program OPTI 1.1 developed for this purpose. As a result, 22 % of the all pre-stressed tendons have been identified that affect this bridge unfavorably, i.e., contribute to an increase of deflection. The tendons located at the bottom surface of the first and third spans (see Fig. 2), prove to be extremely harmful, since all of them enhance the deflections in the central region of the main span. Among the tendons located at the top surface, installed during cantilever erection, the straight ones, which are passively anchored in the vicinity of internal supports and follow the top surface, are harmful. In this particular bridge, the unfavorable tendons in the first, as well as the third, span are anchored typically at distance of approximately 15 m from the ends of the bridge, and the unfavorable tendons inthe main span are anchored typically at distances of approximately 30 m from the mid-span (see Fig. 2).
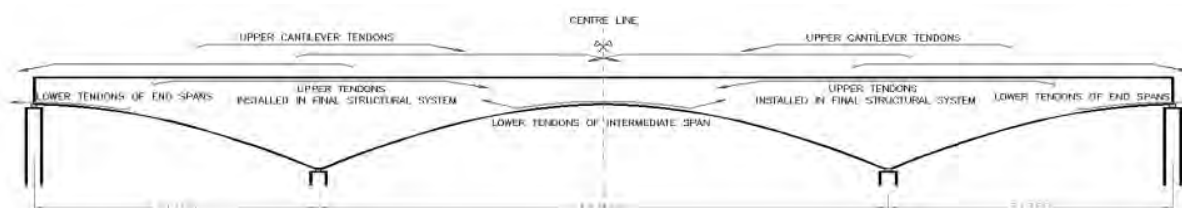
Figure 2: Schematic layout of pre-stressed tendons

3 EXAMPLE OF RECONSTRUCTION

An example is the excessive deflection that required reconstruction of the box girder bridge over river Labe (or Elbe) in Děčín in North Bohemia (Fig. 3). The structural system of this bridge is a three-span continuous box girder (with spans 62.5 + 104+ 62.5 m; Fig. 3). It is tapered in shape and was erected using the cantilever technology.

Figure 3: Bridge over river Labe (or Elbe) in Děčín, Czech Republic

The bridge was monitored since its erection in 1993. The mid-span deflection increased annually by about 8 mm. The total difference between the theoretical and measured road levels reached about 140 mm just before the start of reconstruction. There are several probable reasons for the excessive deflection:

- a lower value of modulus of elasticity of concrete;
- neglect of the shear effect on deflection in the design;
- incorrect compliance function for the evolution of creep in time; and
- a higher influence of relaxation of pre-stressed steel.

In the reconstruction, the stiffness of the structure was increased by adding external pre-stressed tendons, as shown in Fig. 4, 5.

Figure 4: Cross section (Děčín)

Figure 5: View of external tendons (Děčín)

4   CONCLUSIONS

The lesson to be learned from the deflections of the existing bridges is that bridge design should be performed in two different and equally important phases - not only the usual stress analysis, but also the optimization of pre-stressing tendon layout. The latter is a necessity for ensuring acceptable long-term deflections.

5   ACKNOWLEDGMENT

REFERENCES

Křístek, V., Vráblík, L, Bažant, Z.P., Li, G., Yu, Q., 2008. *Mis-prediction of Long-Term Deflections of Prestressed Box Girders: Causes, Remedies and Tendon Layout Effect*, Proc.of Concreep8.

Bažant, Z.P. 2000. *Criteria for rational prediction of creep and shrinkage of concrete. Adam Neville Symposium: Creep and Shrinkage---Structural Design Effects*, ACI SP--194, A. Al-Manaseer, ed., Am. Concrete Institute, Farmington Hills, Michigan, 237-260 (updated from Materials and Structures, RILEM, Paris, Vol. 28, pp. 357-365).

Bažant, Z.P., and Baweja, S. 2000. *Creep and shrinkage prediction model for analysis and design of concrete structures: Model B3. Adam Neville Symposium: Creep and Shrinkage--Structural Design Effects*, ACI SP-194, A. Al-Manaseer, ed., Am. Concrete Institute, Farmington Hills, Michigan, 1-83.

Křístek, V., Bažant, Z.P., Zich, M., and Kohoutková, 2006. *Box girder deflections: Why is the initial trend deceptive? ACI Concrete International* 28 (1), 55-63.

Křístek, V., Vráblík, L., 2007: *Optimization of tendon layout to avoid excessive deflections of long-span pre-stressed concrete bridges*, Concrete Engineering International, Vol. 11, No.1.

Emissions of persistent organic pollutants from transport in the experience of the Czech Republic

V. Adamec[*], J. Dufek, J. Jedlička, R. Ličbinský
CDV – Transport Research Centre, Brno, Czech Republic
* Corresponding author: vladimir.adamec@cdv.cz

V. Bencko
Charles University in Prague, 1st Faculty of Medicine, Institute of Hygiene and Epidemiology, Czech Republic

ABSTRACT: This presentation introduces the situation of POPs transport emissions in the Czech Republic since 1993, including a prediction for the years 2010 and 2015, determination of emission factors, possibilities for their reduction, and legislative framework. From the achieved results it is evident that the emissions from road and railway transport exceeded 28 tons in 2005. The naphtalene creates more than 90 % of emissions of vehicles fulfilling EURO I-III limits. The phenanthrene (about 50 % of PAHs) predominates in emissions of older gasoline vehicles that do not fulfil EURO limits; naphtalene content isabout 10 %. Total emissions of PCDDs and PCDFs are relatively low in the same context ofemissions of mostly older vehicles, manufactured before the acceptance of EURO limits. The potential health risks related to human exposure to transport emissions are the subject of interest of our present research.

KEYWORDS: polyaromatic hydrocarbons, polychlorinated biphenyls, polychlorinated dibenzo-dioxines, polychlorinated dibenzo-furanes, emissions, emission factors, air pollution, transport emissions.

1 INTRODUCTION

Over the past decades transport has become an important factor which affects the environment, both in a positive and a negative way. Besides traffic noise emission, the most serious problem is air pollution, especially due to its effect on human health, particularly in municipalities with dense motor vehicle traffic. Exhaust gases from motor vehicles contain hundreds of chemical substances in different concentrations and with a wide spectrum of potential health effects and related risks to human health (Bencko et al. 1994, 1996). Besides "classical" monitored pollutants, such as nitrogen oxides (NO_X), carbon monoxide (CO), carbon dioxide (CO_2) or sulphur dioxide (SO_2), recent attention has also been paid to human exposure to persistent organic pollutants (POPs) such as polycyclic aromatic hydrocarbons (PAHs), polychlorinated biphenyls (PCBs), polychlorinated dibenzo-p-dioxins (PCDDs) and polychlorinated dibenzofurans (PCDFs).

2 METHODS

With regard to the fact that POPs do not belong to the limited components of the traffic exhaust gases, determination of the emission factors of these pollutants is very limited. The situation is further complicated by the fact that values measured so far have a relatively

large dispersion. The calculation and the audit of the amount of POPs emissions from transport was first stated in the following works: Ntziachristos and Samaras (2000), Krobl (2001) and Adamec et al. (2003a).

The emission factor (Ef) of a pollutant is always presented in the mass per the unit of energy $(g.MJ^{-1})$ʼ the length of transport $(g.km^{-1})$, the mass of consumed fuel $(g.kgfuel^{-1})$ or the power of the engine $(g.kWh^{-1})$. Ef of limited pollutants, such as CO, NO_x, hydrocarbons (C_xH_y), or particular matters (PM), are compulsorily measured (periodical technical inspections), butthe measurement of POPs emissions from transport has so far not been controlled by any legislative directive. This is the reason why POPs emissions from vehicles are not usually measured and these measurements are especially connected with the experimental field. Forthis purpose, the authors made the database of Ef of selected POPs produced by transport (Dufek et al., 2002a). For an increase in the amount of reliable data, the authors performed a measurement campaign, with the collaboration of the Czech Motor Vehicle Research Institute, where the PAHs and dioxins were measured in Czech passenger cars. Results from national and foreign measurements, which are the sources, are continuously updated and evaluated statistically. The following Table 1 presents used emissions factors of selected POPs produced by transport which were used for the elaboration of the emission inventory. Calculations of total emissions used average values for each category of means of transport.

Table 1: Emission factors of selected POPs produced by transport (Dufek & Adamec, 2002a)

Vehicle category	PAH total	PCDD	PCDF
	$\mu g.km^{-1}$	$pg.km^{-1}$	$pg.km^{-1}$
motorcycles	131.64	10.3	21.2
gasoline conventional cars	260.29	10.3	21.2
gasoline cars fulfilling EURO standards	143.84	-	-
diesel passenger cars	1277.44	0.5	1.0
LPG passenger cars	49.46	-	-
gasoline light duty vehicles	378.11	10.3	21.2
diesel light duty vehicles	1601.16	0.5	1.0
diesel heavy duty vehicles	241.86	3.0	7.9

3   RESULTS AND DISCUSSION

For the determination of POPs emissions methodology for the calculation of air polluting emissions from transport was applied (Dufek & Adamec, 2002b) which uses data about the amount of sold fuels. After the deduction of non-transport sources, i.e., diesel fuel consumption in farming, forestry, civil engineering and the army (especially concerning diesel), the amount of sold fuel is split by means of transport performances into particular modes of transport:

- Individual road passenger transport (IPT)
- Public road passenger transport (RPT)
- Road freight transport (RFT)
- Railway transport - motor traction (RWT)
- Waterway transport (WWT)
- Air transport (AIR).

The split of individual fuels is carried out with the help of weighing factors based on transport performances and annual mileages from the national transport statistics. The national traffic census on motorway and road network is the most important and it is carried out once every five years. Transport emissions - producing vehicles are split into

specific categories according to the transport mode, fuel used and equipment with catalytic converters. From this split in consumption, emissions are calculated by means of average emission factors. For each of the given categories the averaged emission factor (g.kgfuel-1) is used, which is based on the measured and statistically processed values. For an elaboration of emission inventory consumptions of particular fuels were used, determined bythe aforementioned methodology and emission factors, presented in Table 1, evaluated statistically in the database of emission factors, and recalculated from g.km-1 to g.kgfuel-1. The emission inventory includes emissions for PAHs, PCDDs, PCDFs, and PCBs.

Emissions from air transport are not included in the aforementioned emission audit because the authors had no access to pertinent data concerning the PAHs in emissions of hydrocarbons produced by combustion of airplane fuels.

Table 2: Total PAHs emissions in the Czech Republic (t)

Mode of transport	Year														
	1993	1994	1995	1996	1997	1998	1999	2000	2001	2002	2003	2004	2005	2010	2015
IPT	6.13	6.64	7.11	8.25	8.54	8.59	9.22	9.45	10.48	10.99	13.03	14.41	16.90	17.34	17.50
RPT	0.33	0.17	0.19	0.20	0.18	0.27	0.27	0.58	0.63	0.66	0.76	0.82	0.95	1.13	1.34
RFT	2.22	3.00	4.00	5.21	5.81	5.16	5.57	6.04	6.68	6.92	8.17	9.04	10.59	11.12	11.24
RWT	0.20	0.16	0.23	0.25	0.21	0.19	0.15	0.10	0.09	0.09	0.09	0.09	0.09	0.08	0.07
WWT	0.03	0.02	0.03	0.04	0.02	0.02	0.01	0.01	0.01	0.00	0.00	0.01	0.01	0.01	0.01
Total	8.91	10.10	11.70	14.12	14.93	14.46	15.22	16.19	17.89	18.66	22.05	24.37	28.54	29.68	30.16

According to our calculations, (Adamec et al. 2003a) the yearly amount of PAHs emissions in the Czech Republic from transport exceeded 28 tons in 2005. The prediction is also quite negative: due to the continuing increase of diesel oil consumption, growth of PAHs emissions is predicted to reach 30 tons in 2015. However, the increase is lower than the supposed traffic increase, because new cars are less pollution-emitting than older ones. The naphthalene creates more than 90 % of PAHs emissions from gasoline vehicles, which meet EURO emission limits, and from diesel vehicles. The phenanthrene (about 50 % of PAHs) predominates in emissions from older petrol vehicles which do not meet EURO emission limits; naphthalene content is less than 10% in the case of these vehicles. We find by comparing PAHs emission factors from various sources that there are not such strong differences between newer and older vehicles as in the case of VOC, because PAHs are not limited by any standards.

Table 3: Total PCDDs emissions in the Czech Republic (mg)

Mode of transport	Year														
	1993	1994	1995	1996	1997	1998	1999	2000	2001	2002	2003	2004	2005	2010	2015
IPT	195.1	214.9	209.6	219.9	211.2	178.1	163.3	116.3	105.6	81.9	77.7	66.1	54.5	52.2	51.4
RPT	3.4	3.7	4.5	4.8	4.5	5.8	5.5	4.4	4.8	4.8	5.6	6.1	7.0	8.1	8.4
RFT	17.9	29.0	32.9	38.1	45.8	37.0	37.0	12.0	13.1	13.1	15.3	16.7	19.3	22.0	22.6
RWT	2.4	2.0	2.9	3.1	2.5	2.6	2.3	1.2	1.2	1.1	1.1	1.1	1.1	0.9	0.9
WWT	0.3	0.3	0.4	0.5	0.2	0.3	0.3	0.1	0.1	0.0	0.0	0.1	0.1	0.1	0.1
Total	219.1	249.9	250.3	266.4	264.2	223.8	208.4	134.0	124.8	100.9	99.7	90.1	82.0	83.3	83.4

Table 4: Total PCDFs emissions in the Czech Republic (mg)

Mode of transport	Year														
	1993	1994	1995	1996	1997	1998	1999	2000	2001	2002	2003	2004	2005	2010	2015
IPT	403.2	444.4	433.3	454.6	436.6	368.2	338.0	240.2	218.1	169.0	160.3	136.2	112.1	107.2	105.6
RPT	4.9	4.2	5.1	5.3	4.9	6.3	6.1	4.4	4.8	4.8	5.6	6.1	7.0	8.1	8.4
RFT	32.8	54.7	61.3	69.9	84.5	67.6	80.0	12.0	13.1	13.1	15.3	16.7	19.3	22.0	22.6
RWT	2.4	2.0	2.9	3.1	2.5	2.6	2.3	1.2	1.2	1.1	1.1	1.1	1.1	0.9	0.9
WWT	0.3	0.3	0.4	0.5	0.2	0.3	0.3	0.1	0.1	0.0	0.0	0.1	0.1	0.1	0.1
Total	443.6	505.6	503.0	533.4	528.7	445.0	426.7	257.9	237.3	188.0	182.3	160.2	139.6	138.3	137.6

PCDDs and PCDFs emissions from transport reach totally milligrams. They are mostly produced by older vehicles which do not meet EURO 1-3 emission limits. The downward trend in the production of these emissions from transport is caused by renewal of the vehicle fleet, especially in the individual road passenger transport. From the COPERT database of emission factors it is not possible to ascertain if these emissions from older vehicles are fixed on the halogenated scavengers or if they originate from trace amounts of chlorine in the petrol.

Emission factors of PCDDs and PCDFs are very low, in $pg.km^{-1}$, and hence it is also probable the origin of this minimum amount is by burning fuels which do not contain halogenated scavengers. This assumption is also supported by the fact that the database includes emission factors of diesel vehicles as well, where halogenated ingredients were not applied. Nevertheless a suspicion that polyhalogenated hydrocarbons from exhaust emissions can contribute to a total human exposure to this kind of xenobiotics was raised from results of the analyses of breast milk samples collected at places with extremely high traffic density (Bencko et al. 2004).

Table 5: Total PCBs emissions in the Czech Republic (mg) – gasoline vehicles

Mode of transport	Year														
	1993	1994	1995	1996	1997	1998	1999	2000	2001	2002	2003	2004	2005	2010	2015
IPT	169.0	190.1	192.4	212.0	218.8	204.7	224.4	226.5	222.4	218.2	237.7	235.5	231.3	216.9	212.6
RPT	0.3	0.4	0.4	0.4	0.3	0.4	0.4	0.4	0.5	0.6	0.7	0.8	0.9	1.1	1.3
RFT	10.0	17.5	19.1	21.2	26.0	20.3	24.7	26.1	26.9	31.3	28.4	28.2	27.5	25.6	24.9
RWT	0.1	0.1	0.1	0.1	0.1	0.1	0.1	0.1	0.1	0.1	0.1	0.1	0.1	0.1	0.1
WWT	0.0	0.0	0.0	0.0	0.0	0.0	0.0	0.0	0.0	0.0	0.0	0.0	0.0	0.0	0.0
Total	179.4	208.1	212	233.7	245.2	225.5	249.6	253.1	249.9	250.2	266.9	264.6	259.8	243.7	238.9

Note: PCBs emissions were calculated only for gasoline vehicles because no measurements of emission factors of PCBs of diesel vehicles were found.

4 CONCLUSIONS

POPs emissions from mobile sources are high due to the large proportion of older vehicles on the road in the Czech Republic. Only their replacement by up-to-date vehicles, equipped with suitable technologies for the reduction of POPs, will contribute to a decrease in their total production.

The PAHs and POPs emissions are a part of the total hydrocarbon emissions that are limited by UN ECE standards. The PAHs themselves are not limited by any specific emission standard or environmental limit and so their emissions are not regularly checked. Their significant increase in the Czech Republic was detected in 1993 and has continued up tothepresent day. This fact represents a threat to air quality and demonstrates the increase ofthe potential adverse impact of traffic emissions on human health.

Our main health interest in a current project dealing with solid aerosols in traffic emissions is oriented due to our previous experience (Bencko & Reichrtová, 1992; Reichrtová & Bencko, 1996) on immunity aspects in this context.

REFERENCES

Adamec, V., Dufek, J., Jedlička, J., Cholava, R., 2003a. *Persistent organic pollutants in transport sector.* In. Robert Joumard. 12th Symposium "Transport & Air pollution" volume 2. Arcueil: INRETS, p. 209 - 212. ISBN 2-85782-588-9.

Adamec, V., Dufek, J., Huzlík, J., Cholava, R., Jedlička, J., Klustová, P., Marešová, V.,Šucmanová, M., 2003b. *Research of Environmental Burden from Transport.* Brno: CDV, 200 p. (In Czech).

Bencko, V. & Reichrtová, E., 1992. *Immunological Aspects of Exposure to Exhaust Gases.* In: Proc. International Workshop on Human Health and Environmental Effects of Motor Vehicle Fuels and their Exhaust Emissions, Sydney, Australia, pp. 185-191.

Bencko, V., Tuček, M., Volný, J., 1994. *Health Aspects of Human Exposure to Exhaust Gases.* In: Proc. XIV Asian Conference on Occupational Health. Beijing, China: pp. 423.

Bencko, V., Šuta, M., Tuček, M., Volný, J., 1996. *Health Aspects of Human Exposure to Oxidants and Exhaust Gases.* In: Proc. Indoor Air 1996, Nagoya, Japan: pp. 1137-1142.

Bencko, V., Černá, M., Jech, L., Šmíd, J., 2004. *Exposure of Breast-fed children in the Czech Republic to PCDDs, PCDFs, and Dioxin-like PCBs.* Environmental Toxicology and Pharmacology, vol.18, pp. 83-90.

Dufek, J. & Adamec, V., 2002a. *Database of Measured Emission Factors from Transport Sector.* CDV, Brno, Czech Republic (In Czech).

Dufek J. & Adamec, V., 2002b. *Methodology of the Calculation of Air Polluting Emissions for All Transport Modes.* CDV, Brno, Czech Republic, 24 p. (In Czech).

Krobl L., 2001. Survey of Emission Factors of Road Motor Vehicles. ÚVMV, Prague, Czech Republic, 35 p. (In Czech).

Ntziachristos L. & Samaras, Z., 2000. *COPERT III - Computer Programme to Calculate Emissions from Road Transport.* Methodology and Emission Factors (Version 2.1). EEA, Copenhagen, Denmark, 84 p.

Reichrtová, E. & Bencko, V., 1996. *Immune Response to Exhaust Gases Derived from Two Cycle Combustion Engine Following Experimental Exposure.* Centr. eur. J. publ. Health, vol.4. pp 4-10.

USEPA, 2000. *Exposure and Human Health Reassessment of 2,3,7,8-Tetrachlorodibenzo-p-Dioxin (TCDD) and Related Compounds.* Part I: Estimating Exposure to Dioxin-Like Compounds. Volume 2: Sources of Dioxin-Like Compounds in the United States. (draft) [online]. Accessible on site http://cfpub.epa.gov/ncea/cfm/part1and2.cfm?ActType=default (cit. 2005-May-11).

USEPA, 2001. *Database of Sources of Environmental Releases of Dioxin-like Compounds in the United States.* Version 3.0. (EPA/600/C01/012) [online]. Accessible on site http://cfpub.epa.gov/ncea/cfm/dioxindb.cfm (cit. 2005-05-11).

WHO, 2000. *Guidelines for air quality.* Geneva, Switzerland, WHO.

WHO, 2000a. *Air Quality Guidelines for Europe, Second Edition.* Regional Publications, European Series, No. 91. Geneva, Switzerland, WHO, 288 p., ISBN 92-890-1358-3.

Human body finite element model as an instrument for the improvement of passive safety

L. Číhalová[*] & L. Hynčík

New Technologies Research Center, University of West Bohemia, Plzeň, Czech Republic
* Corresponding author: cihalin@ntc.zcu.cz

ABSTRACT: Recently the virtual finite element human body models have become important when used to improve the passive safety of vehicle occupants. The human body models have a significant advantage over dummies, since they are able not only to predict injuries, but also to model the whole injury mechanism. This enables the detailed analysis of injuries, and hence a more precise optimization of safety systems. To be able to use the models for this purpose, an objective model of the human body needs to be created. Such a human body model, ROBBY, is being developed at the University of West Bohemia (UWB) in cooperation with the ESI Group. This model is still being updated to be a more realistic model. The aim of this study was to improve the thoracic part of the human body model by the implementation of a created thoracic model to the existing ROBBY model and use the updated model as a tool for safety evaluation. Two types of sled tests were performed to compare the behavior of the updated model ROBBY and cadavers. The first sled test was performed at 30 km/h without airbag, and the second at 50 km/h with airbag. A comparison of the response of the thorax-abdomen complex for the model and cadavers was performed.

KEY WORDS: Sled test, ROBBY model, cadaver, biomechanics, frontal impact

1 INTRODUCTION

In the European Union, the assessment of the protection offered by a vehicle to a restrained occupant in the case of a collision is based on biomechanical data measured on the HYBRID III crash test dummy, as described by the European Frontal Directive (Directive 96/79/EC). Our presented study is based on the paper of (Vezin et al., 2002), who obtained new biomechanical data of the behavior of the human thorax/shoulder complex under different frontal impact conditions.

  Since the response of the human body during various accidents is still the objective of much research, our endeavor is to have a more realistic model of the human model ROBBY developed in UWB in cooperation with the ESI Group, see (Hynčík, 2002). The aim of the presented study was to improve the previously developed model ROBBY in the sense of the integration of a created thoracic model into the model as a whole. To check the reality of the response of the thoracic part of the updated ROBBY model, two types of sled tests were performed. The response of the ROBBY model was compared with the response of cadavers according to (Vezin et al., 2002). The main goal of the study was to show the possibility and advantages of using human body models in virtual safety systems design.

2 PREPARATION OF THE MODEL

(Číhalová, 2006) previously created and validated the FE model of the thorax (see Figure 1), whose geometry was based on the Visible Human Project photographs, see (VHP, 2003). This model was consequently scaled, and further it was embedded into the complete human body model ROBBY, see Figure 2. The ROBBY model represents an average adult male. This model belongs to the ROBBY family, which consists of ROBBY2 – a model of a man (on various levels), ROBINA – a model of woman, and BOBBY6 – a model of a child. The family is multi-body-based. The ROBBY model enables the detailed description of impact consequences, since there are modular implementations of a deformable abdomen and thorax. Modular means that a rigid part can be substituted with a deformable one.

**Figure 1: The developed thoracic model, old
and updated thorax-abdomen complex of ROBBY model**

Figure 2: ROBBY model

3 FRONTAL SLED TEST

The laboratory sled tests have been designed to simulate the inertial effects of real vehicle frontal crashes. Generally, the sled test studies are useful for understanding the occupant kinematics and the injury mechanisms according to the restraint systems. In the past, many frontal sled tests have been performed with different subjects seated in the driver position and different restraint conditions by (Kallieris et al., 1995), (Kleinberger et al., 1998), etc. In this study, the sled tests were simulated according to (Vezin et al., 2002). He performed

sled tests in LBMC (Laboratoire de Biomécanique et de Mécanique des Choes); and tests are similar to those used at the University of Heidelberg by (Kallieris, 2001). In Vezin's study, two series of tests with Post Mortem Human Subject (PMHS), Hybrid III and Thor-α dummies were conducted.

The first series of tests according to (Vezin et al., 2002) were performed at a lower velocity, 30 km/h, with a 15 g peak sled deceleration pulse (see Figure 3), using a lap belt and a shoulder belt. The second test was performed at a higher velocity, 50 km/h, with a higher deceleration pulse of about 22 g (see Figure 3), and a restraint system composed of a lap belt, a shoulder belt and an airbag. These deceleration laws were chosen in order to evaluate the responses of the dummies under such impact conditions that can lead to no, or low, injuries risk.
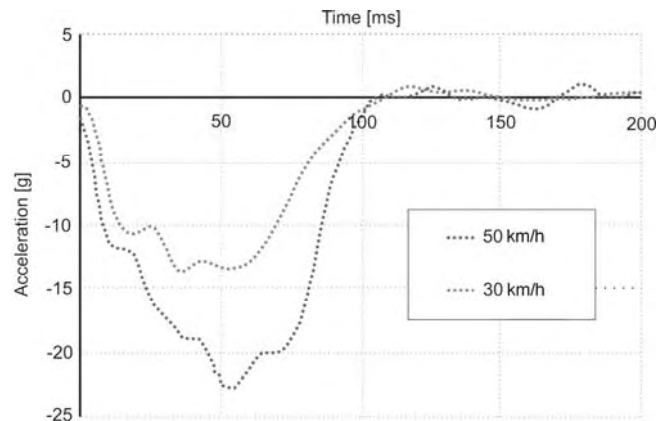

Figure 3: The sled deceleration time history according to (Vezin et al., 2002)

To simulate these tests, the seat geometry was chosen to correspond to a standard mid-sized car. The seat pan had a slope of 18° and the footrest a slope of 43°. The feet of the surrogate were strapped to the footrest. The seat was rigid. The model was restrained using a three point belt system and, in case of the 50 km/h test, by the airbag. The belt restraint system includes a retractor, force limiter and a slip-ring between the shoulder belt and the lap belt. The setup of sled tests is visualized below, see Figure 4.
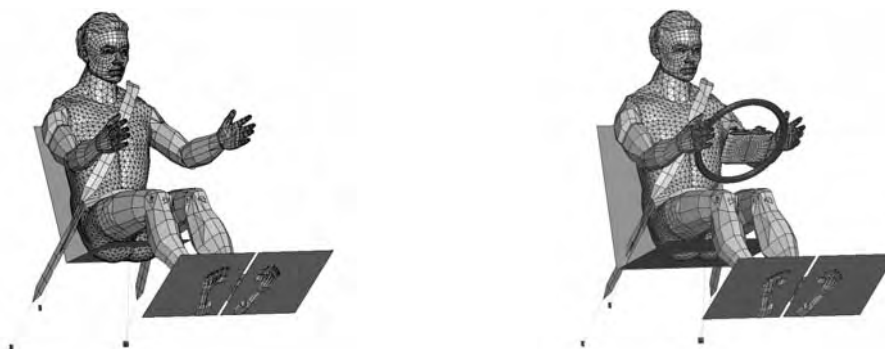

**Figure 4: The setup of sled tests: at lower velocity without airbag (30 km/h test)
and at higher velocity with airbag (50 km/h test)**

The time dependencies of T1, T8, T12, lower and upper sternum accelerations; and the shoulder and lap belt load time history were investigated to compare the behavior of the updated ROBBY model with the behavior of cadavers investigated by (Vezin et al., 2002). All investigated dependencies were filtered by CFC60, see (PAM-CRASH/SAFE^{TM}, 2007).

3.1   BELT LOADS

Figure 5 represents shoulder belt load time histories for the 30 km/h and 50 km/h tests. The load in the shoulder belt rises rapidly from 30 to 75 ms. The force-limiting system enters the play after 75 ms for the 50 km/h test and the load is sustained for approximately 10 ms. After this time the load declines. For the 30 km/h test without airbag, the load limit of 4 kN is not reached. As can be seen from Figure 5 the simulation results are in agreement with experimental results. The lap belt loads for both tests are presented in Figure 6.
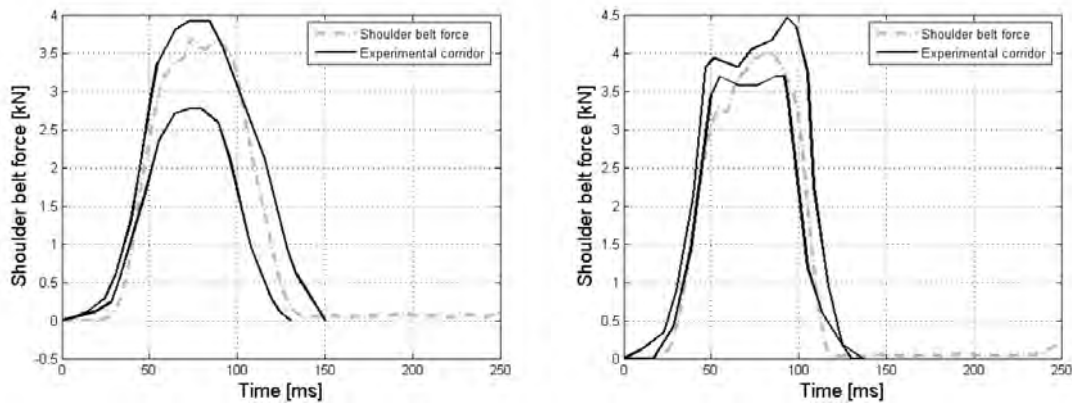
Figure 5: The shoulder belt load time history for the 30 km/h test and the 50 km/h test
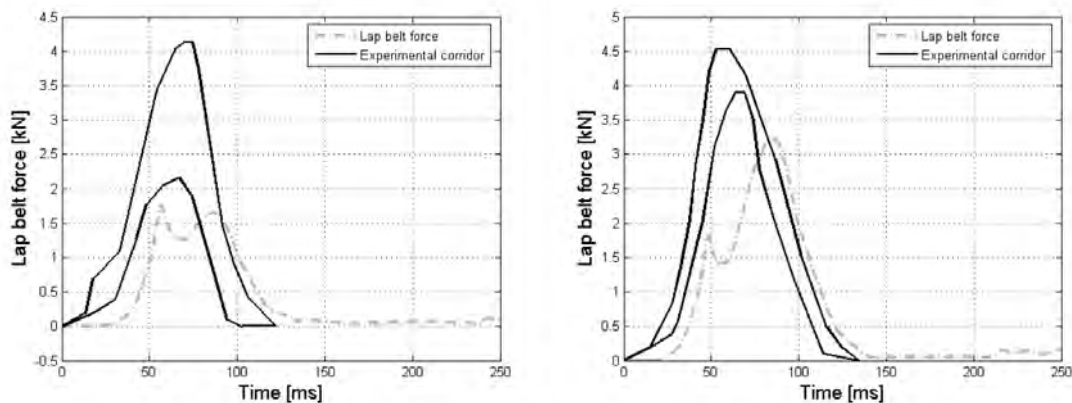
Figure 6: The lap belt load time history for the 30 km/h test and the 50 km/h test

The results of lap belt loading are in agreement with reality in the phase of unloading. During the phase of loading the simulation lap belt load is smaller than experimental one. This could have been caused by the response of the abdomen; it seems that it is softer than the real abdomen. Hence, there arises the necessity to improve this part of ROBBY model in the future.

3.2   THORACIC SPINE ACCELERATION

The behavior of the thoracic spine can be investigated through the dynamics of the T8 and T12 vertebrae. Results of the simulation for both tests show two peaks, see Figure 7 and 8. However, in the case of the 30 km/h test without airbag the second peak is lower than the first one. In the case of the 50 km/h test with airbag the second peak is comparable with the first one. The first peak of the 50 km/h test at 50 ms corresponds to the load

of the thorax by the shoulder belt and the second peak at 80-90 ms arises as a consequence of the load of the chest by the airbag.
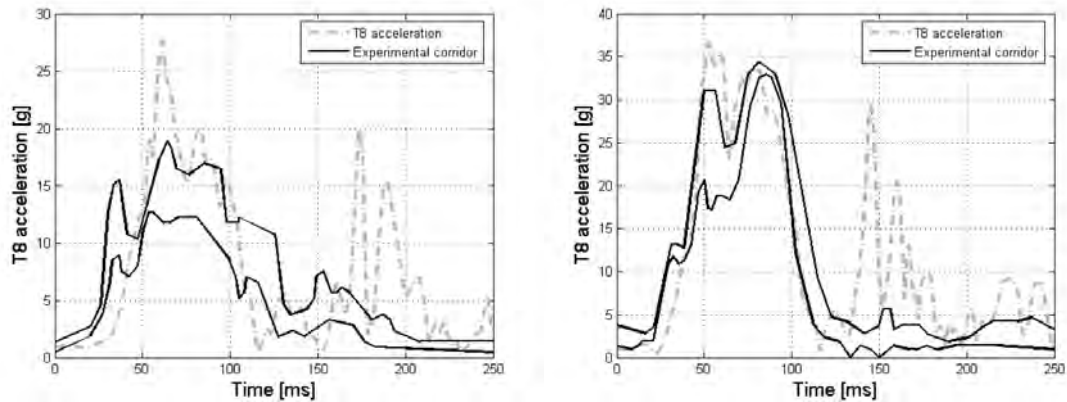

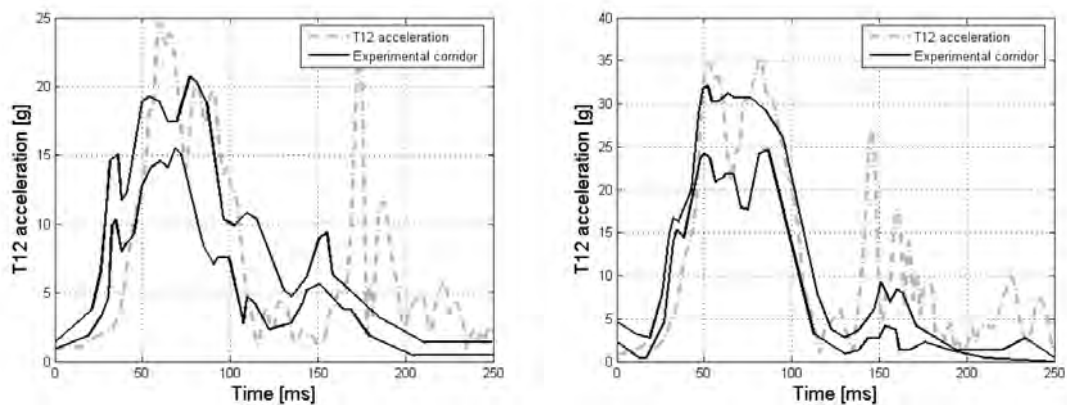**Figure 7: The T8 resultant acceleration time history for 30 km/h and 50 km/h tests**

Figure 8: The T12 resultant acceleration time history 30 km/h and 50 km/h tests

At the beginning, the accelerations for both tests rise rather slightly compared with the accelerations of cadaver. During the 30 km/h tests the peaks of accelerations around 60 ms are a little higher than those of the cadavers. However, in the increase and decline phase the results are comparable.

3.3   UPPER SPINE ACCELERATION

The upper spine behavior can be studied through the dynamics of the T1 vertebra. T1 accelerations for both tests are visualized in Figure 9.
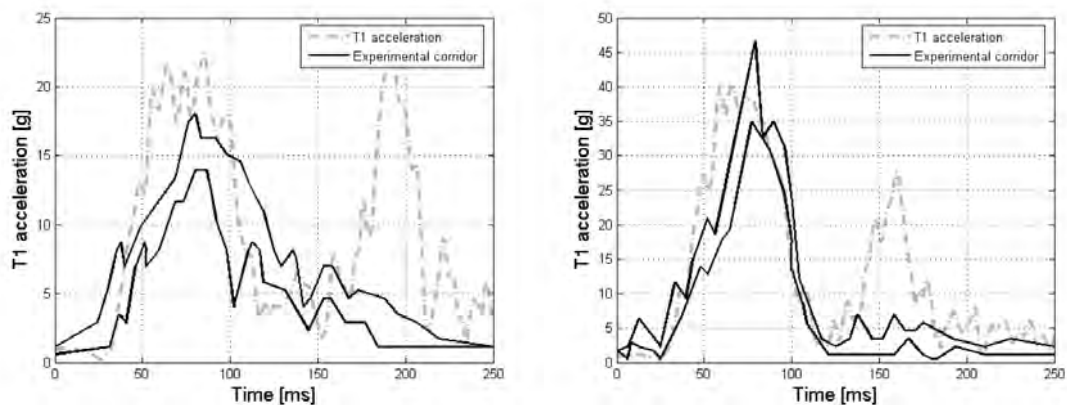

Figure 9: The T1 resultant acceleration time history for 30 km/h and 50 km/h tests

The accelerations in the 30 km/h test rise above the acceleration of the experiment. However, in the case of the 50 km/h test, the acceleration of the model corresponds to the response of the cadaver.

3.4 STERNUM ACCELERATION

Although the T1 corresponds to the upper sternum and T8 corresponds to the lower sternum in a geometrical way, their accelerations are rather different, see Figure 7, 9, 10 and 11.
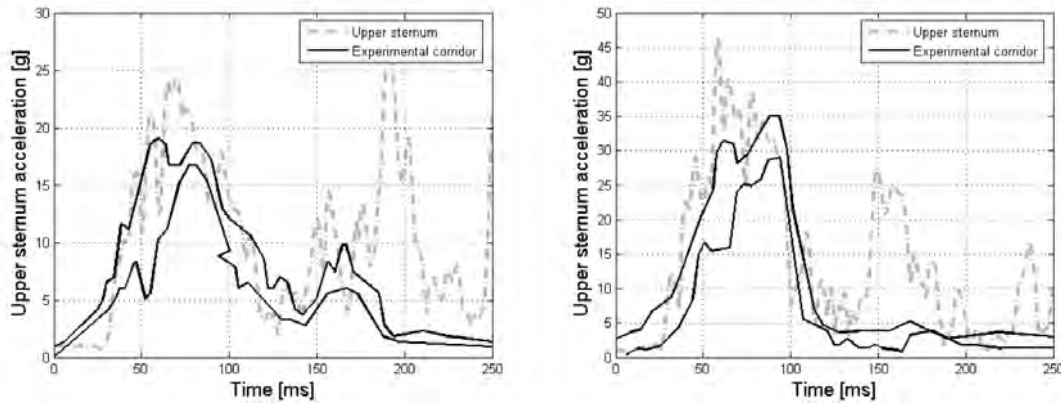

Figure 10: The upper sternum resultant acceleration time history for the 30 km/h and 50 km/h tests
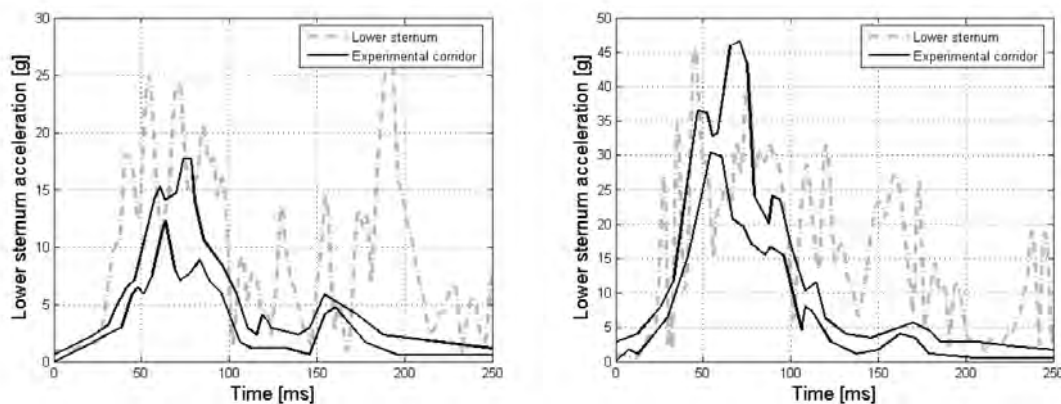

Figure 11: The lower sternum resultant acceleration time history for the 30 km/h and 50 km/h tests

The increase and decline phases of upper sternum accelerations in both tests are in agreement with experimental results. Only the first peak of acceleration is a little higher than the experimental one, see Figure 10. In the case of lower sternum acceleration more dissimilarities can be observed, see Figure 11. This could be caused by the problem with abdomen and the fact that the response of the lower sternum is influenced by the abdomen. However, in both test results it can be seen that the trend function of both results is similar to the experimental one.

In summary, all results agree with the experimental ones. Hence the simulation results belong to the corridors or are close to them. The first peaks of all simulation results are rather higher than the experimental ones. This is influenced by the properties of restraining systems.

Consequently, other peaks are evident around 150 ms in all results. These correspond to the interaction of the body with the seat.

3.5   RIBCAGE ACCELERATION

Figure 12 represents the accelerations of the 4th and 6th rib (left and right) at 30 km/h without airbag, and at 50 km/h with airbag. The direction of the measured acceleration (one component) was perpendicular to the rib, hence measured in the X axis according to (Vezin et al., 2002).
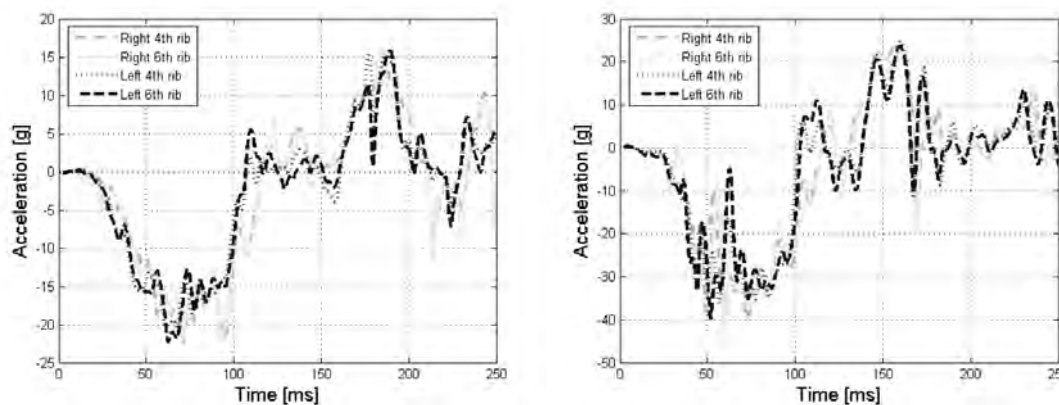

Figure 12: Rib acceleration X time history for the 30 km/h and 50 km/h tests

There was no significant difference between the accelerations of 4th and 6th rib on the left and right side. At 30 km/h the deceleration was faster on the left ribs than on the right ribs, which indicates a greater chest deflection on this side. At the 50 km/h the thorax is deformed on the left side only a little more than on the right side and therefore the difference between individual accelerations is not so appreciable.

4   INJURY INVESTIGATION

The great advantage of the ROBBY model is its ability to predict injuries sustained during traffic accidents. The often used injury criteria (Schmidt et al., 2004) such as HIC (Head Injury Criterion) (see Table 1) for head, compression C, rate of deformation V, rate of compression VC for thorax and abdomen, acceleration of spine and loading of sternum can be investigated on this model. Moreover, since the thoracic part of the ROBBY model was modeled as deformable, it allows a view of the deformation of internal organs, such as lungs, heart and aorta and bony parts, such as sternum, ribs and vertebrae.

Table 1: The evaluation of HIC for ROBBY and comparison with results according to (Vezin et al, 2002).

	30 km/h test	50 km/h test
Cadaver	160	620
Hybrid III	86	230
Thor-α	107	427
ROBBY	132	774

5 CONCLUSION

The aim of this study was to integrate the created and validated model of the human thorax into the previously developed model ROBBY presenting a model of the average adult male. The reality of the updated model was validated by virtue of two types of sled tests according to (Vezin et al., 2002). The response of the thorax model was compared with the response of the cadaver thorax. The results of the comparison show that the updated model ROBBY is a satisfactory approximation of the human body. There are some deviations visualized by the peaks after 150 ms in all the results. However, these deviations occur after the unloading phase and they could have been caused by the bad interaction of the model with the back seat. This suggests the objective for the following improvement of the ROBBY model, i.e., to improve the deformable model of the abdomen and to validate it in the future, using the sled test. In conclusion, the updated model is a very good approximation of the human body and moreover it has the ability to predict injuries. Therefore, its continued usage in virtual safety systems design could be possible.

6 ACKNOWLEDGEMENT

REFERENCES

Číhalová, L, 2006. *Development of biomechanical deformable thoracic model*, Journal Engineering mechanics, vol. 13, No. 6, pp. 453-465.

Directive 96/79/EC of the European Parliament and of the Council of 16 December 1996, on the protection of occupants of motor vehicles in the event of a frontal impact. Directive 199/98/EC, Amendment 15 December 1999, Official Journal of the European Communities, Brussels.

Hynčík, L., 2002: *Biomechanical model of abdominal organs and tissue for car crash test purposes*, Ph.D.Thesis, University of West Bohemia, Plzeň.

Kallieris, D., 2001: *Personal communication*, University of Heidelberg, Germany.

Kallieris, D., Rizzeti, A., Mattern, R., Morgan, R., Eppinger, R., and Keenan, L., 1995. *On the synergism of the driver air bag and the 3-point belt in frontal crashes*, Proceeding 39th Stapp Car Crash Conference, pp. 389-401.

Kleinberger, M., Sun, E., Eppinger, R., Kuppa, S., Saul, R., 1998. *Development of Improved Injury Criteria for the Assessment of Advanced Automotive Restraint System*, NHTSA report.

PAM-CRASH/SAFE [TM], *Notes Manual*, Version 2007.

Vezin, P., Bruyere-Garnier, K., Bermond, F., Verriest, J. V., 2002. *Comparison of HYBRID III, Thor- α and PMHS Response in Frontal Sled Tests*, Stapp Car Crash Journal, vol. 46, pp. 1-26.

Schmitt, K.U., Niederer, P., Walz, F., 2004. *Trauma Biomechanics*, Introduction to Accidental Injury, Springer, Zurich.

Visible Human Project (VHP), U. S. National library of medicine, 2003.

Load rating assessment of masonry arch bridges

P. Řericha[*]
Czech Technical University in Prague, Faculty of Civil Engineering, Czech Republic
* Corresponding author: rer@cml.fsv.cvut.cz

ABSTRACT: Simple formulas are developed for the mass scale load rating assessment of masonry arch bridges in terms of four geometrical parameters of the bridge. The ultimate load limit state and the repeated load limit state constitute the theoretical background. The formulas are constructed as the minimum squares best suited to a set of linear and non-linear finite element solutions of a representative selection of the country's bridge stock. The formulas are quadratic in the arch span and linear in the arch rise, arch thickness and fill depth. The method can be used for other countries' masonry arch bridge stock; the data processing programme is portable. The structure of the formulas and the country's bridge stock representation can be adapted to local conditions. Nevertheless, new representations of bridge instances require rather demanding non-linear finite element solutions up until total collapse. This is the most laborious part of the formula's development.

KEY WORDS: Arch bridges, masonry, load rating, limit states, finite element method, semi-empiric formulas

1 INTRODUCTION

Load rating of masonry arch bridges is important for road maintenance and management. Its economic impact is considerable, owing to the large numbers of these structures in all developed countries. For the same reason, the assessment methods should be simple and applicable on a mass scale. Also, inevitable uncertainties in material properties make the use of sophisticated analytical methods disputable. The Czech Ministry of Transport therefore funded the development of a manual for the load rating of the country's masonry arch bridges, referred to as the Guide in the paper. The Guide is designed for local bridge engineers with standard civil engineering education and practice. The simplicity requirement admits only semi-empirical formulas. Pippard's formula, (Pippard 1938), see also Heyman (1982) became the basis of the MEXE load rating method, devised in the 1950s in a British military experimental establishment, which in turn has been adapted to several guides and is widely used today, (Highway Agency 1997, UIC 1995 and Min. of Transport CR 2000). Failure criteria play an important part in the development of semi-empirical formulas. The middle half rule is accommodated in Pippard's formula, whereas a relative thrust line eccentricity of 0.35 is allowed in Czech assessment tables, (Min. of Interior CR, 1989). A common deficiency of approximate methods and formulas is that the interaction of the barrel, fill, abutments and roadway is not properly accounted for. As for the analytical methods, the greatest effort has been directed toward the accurate simulation of ultimate limit load states (ULS) and bridge collapse, see (Owen 1998, Fanning, Boothby, Roberts 2001 and Fanning, Boothby 2003) among others. The load rating, i.e., the load capacity for service conditions, is then derived as a fraction of the ultimate limit load. Probably the most advanced and cited British design manual, Highway Agency (2001), recommends a safety

factor of γ =3.4, whereas, when the standard structural reliability factors of Eurocodes are combined, the reduction factor is 2.17. The latter value applies to the ultimate load based on characteristic values of material strengths and no dynamic factor is included. The nature of the typical collapse, namely, the stability loss when four virtual hinges arise, see (Highway Agency 2001), does not admit the standard partial safety factor approach. A consistent probabilistic reliability theory fails, too, since necessary stochastic data is missing. The reduction of the ultimate load to the load rating for the service load is speculative and uncertain. Two concepts are utilized in the Guide development in order to reduce uncertainty.

First, the ULS is not the only limit state from which the load rating is derived; a repeated load limit state (RLLS) is introduced. Second, the safety factor in the ULS is calibrated by comparison to other load rating methods. The Guide features these basic concepts:

1. The load rating method and structure models do not account for abutment, piers and foundation compliance and failure. These structural parts require individual treatment that can hardly be condensed in a common guide.

2. Two limit states, the ULS and the repeated load limit state (RLLS), defined below, determine the load rating.

3. Simple semi-empirical formulas are derived as minimum squares best suited to a set of numerical finite element linear and non-linear solutions of a representative set of bridge instances termed the *representation*.

4. Besides the direct semi-empirical formula for the load rating, criteria are provided for an elaborate assessment by *linear* numerical analysis. Their limit values follow from semi-empirical formulas as well.

5. The two methods developed for the load rating, the direct semi-empirical formula and numerical analysis, are hierarchical as to their precision, work load and use.

2   REPEATED LOAD LIMIT STATE

In practice, most bridges are put out of service when excessive deterioration of masonry occurs, particularly deterioration of the joints. This can be considered another limit state which belongs to the serviceability limit states in the CEN ENV 1991-1 1994 nomenclature. The associated limit load is a repetitive vehicle passage that does not induce cumulative persistent damage in the bridge structure. Experience shows that moderate cracks in the barrel can stabilize. The existence of cracks alone therefore is not a suitable criterion of the limit state. The relative crack depth c_0 (with respect to the arch thickness) is adopted herein for the quantity to compare in this limit state. It is assumed that a crack depth limit $c_{0,lim}$ exists for 'harmless' cracks, an analogy to the endurance limit in fatigue. Unfortunately, sufficient experimental evidence on $c_{0,lim}$ will not be available in the foreseeable future. Despite this, the *repeated load limit state* (RLLS), is adopted for the second limit state in the project. The limit crack depth is determined by calibration and expert agreement, which is common practice in design standard criteria selection. Note that non-linear structural analysis is indispensable for the RLLS solution in spite of the fact that it is a serviceability limit state.

Recently, Melbourne et all (2007) proposed a similar limit state, the permissible limit state (PLS). The purpose of the PLS is similar. It is also unique for masonry arch bridges and should be additionally checked with the standard ultimate load limit state. Its definition is "the limit at which there is a loss of structural integrity that will measurably affect the ability of the bridge to carry its working loads for the expected life of the bridge". Criteria of the PLS depend on the failure mode and are not definitely specified in the paper.

The authors present an example in which the criteria are the endurance limit compressive stress in bending and the longitudinal shear stress between rings in rings separation. The former is one half of the compressive strength with vague justification, the latter was determined from a series of laboratory tests (0.1 Mpa). It is difficult to imagine how the endurance limit shear stress could be determined for an existing bridge. Nevertheless, the paper indicates the need for a specific limit state for masonry arch bridges.

3   PARAMETER RANGES AND THE BRIDGE POPULATION REPRESENTATION

The ULS and RLLS are difficult to account for in simple assessment formulas. The approach adopted herein is based on numerical linear and non-linear solutions of the representation and their best fit approximation by the target semi-empiric formulas. Prospective users of the formulas need not know about the subtleties of the non-linear numerical solutions. Semi-empiric formulas must have applicability ranges specified on their parameters, which should cover the country's bridge population as much as possible. A survey of masonry arch bridge stock in the country has been conducted with a statistical assessment of their parameters. On this basis, a decision has been made on the ranges of the parameters to be covered by the target formula and by the representation. The outcome ranges of the geometrical parameters

$$2<l<8[m], \qquad 0.15<h/l<0.5, \ 0.07<d/l<0.20, \qquad 0.08<s/l<0.45$$

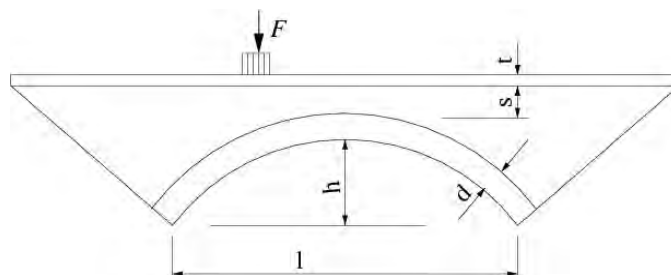cover 95% of the country's stock. Parameters are shown in Fig.1.

Figure 1: Schematic longitudinal section, method parameters

The parameter ranges govern the selection of bridge instances to be included in the representation and analysed. The survey did not identify any multi-ring arches so ring separation is not considered in the representation analyses. The results presented herein are based on a representation including 37 instances. They do not quite regularly cover the four-dimensional space of parameters (three values per parameter mean 3^4=81 instances). Convenience of mesh generations and similar aspects play a part in the instances selection. The representation is displayed in Fig. 4. The format of the instance legends is *l-h-d-s*. Note that absolute lengths are used in the legends.

4   FINITE   ELEMENT   LINEAR   AND   NON-LINEAR   SOLUTIONS OF THE REPRESENTATION, BRIDGE STRUCTURE AND LOAD MODELS

A simple target formula demands a simple structure model. It is assumed that load carrying capacity depends mainly on the longitudinal bridge section. A *plain strain 2D* structure model is therefore sufficient to disclose the principal dependencies. This does not preclude 3D

analyses of individual structures as options in the numerical method (see section 6). Properties and parameters associated with the cross-sections of the bridges are included 'ex post' in approximate corrections if necessary.   This approach is rather common in theoretical and experimental bridge load capacity assessments and load rating methods since it saves full 3D analyses. A schematic longitudinal section of the bridge in Fig. 1 exposes the bridge parameters to be represented in the target formula, barrel span l, barrel rise h, barrel thickness d, and fill thickness s above the barrel crown. These parameters appear in the mathematical formulation of the best fit problem specified in section 5. The inclination of the fill wedges was approximately the same for all representation instances. The wedges provide approximately correct boundary conditions for the fill volume above the arch that takes part in the live load transition. They are fixed at the external (lower) boundaries and so are the ends of the arch. An average thickness t=0.15 m is assumed for the roadway.

Material models and constants are the same in the whole representation, see Table 1, and do not appear as variables in the formulas. This seems to be too radical an assumption, since the bridge load rating does not depend on the properties of the materials. Nevertheless, it has been used several times already, by Heyman (1982) and Fanning & Boothby (2003). The failure criteria of four bridges assessed in (Boothby, 2001) deliver the same results regardless of material strengths. These references testify that the assumption is acceptable. However, the main reason for its adoption is that material constants are not available for the formula's users. In routine applications, an engineer has only the results of a visual inspection with no quantitative data on material properties. A proper probe by (mostly) non-destructive methods would often cost more than the bridge itself.

For simplicity and easy comparison with foreign solutions, no tension material is assumed in the arch. The barrel in plain strain conditions can be modelled by 2D elements or by shell elements which reduce it to a 1D continuum.

Three FEM non-linear packages have been used. Most computations have been done by Adina R&D, (2004), several results checked with Atena by Cervenka Consulting, (2007) and with an in-house code by Rericha, (2000), using the mesh generator by Rypl, (2004). All three packages feature similar material models and finite element types. A difference worth mentioning is that the third package supports layered shell elements with a suitable material model whereas in the first two, isoparametric 2D elements are used for the arch. The distorted mesh is shown in Fig. 2 prior to collapse for an instance of the representation. The cracked parts of the joints are indicated and plastic strain contours in the fill are displayed.

Important restrictions are made on the live load variability. With regard to the barrel span bounds eq. (1), the moving vehicle is reduced to a single axle (the rear axle of a truck) in a lane. Further, a single position of the axle in the span direction is considered at 1/4 of the barrel span. If full variability of the live load were considered according to most standards, the determination of limit states would become unmanageable. Reduction to 2D plain strain conditions entails the replacement of the actual axle pressure pattern by a uniform pressure strip in the lateral direction. The pressure strip is indicated by the double force in Fig. 2. Most papers cited in the introduction section adopt a similar live load proxy.
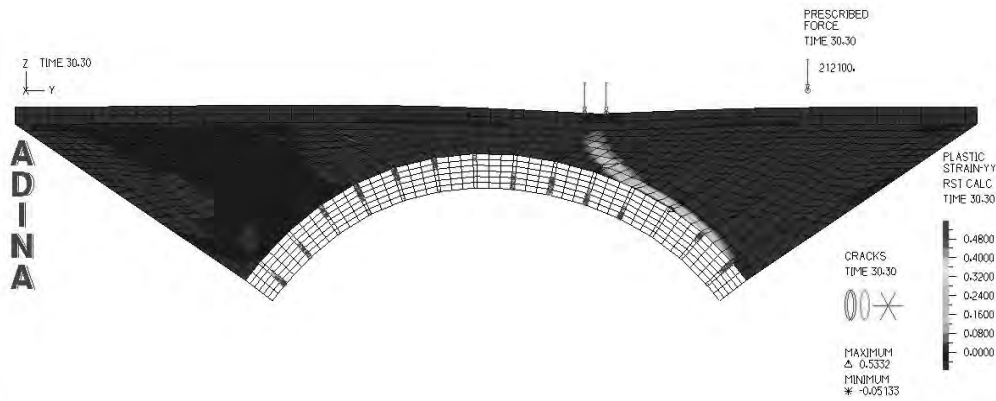
Figure 2: Finite element mesh, plastic zone in the fill and cracks in the arch joints at the ultimate load level for an instance bridge

Tab. 1: Material models and constants, units *m, t, s, kPa*

	Young modulus	*Poisson ratio*	*density*	*compr. strength*	*tension strength*	*cohesion*	*friction angle*	*yield stress*
arch	3.0+06	0.15	2.0	-3000.	10.			
fill, Mohr Coulomb	4.0+4	0.30	1.7			10.	0.50	
roadway, Mises	5.5+06	0.20	2.0					6000.

Table functions ej(f) and c0,j(f) are recorded from the linear and non-linear analyses of each instance j where f denotes the load factor for the live load, ej(f) is the maximum relative thrust eccentricity in the linear solution of the instance j and c0,j(f) is the maximum relative crack depth in the non-linear solution. Maximum within the arch is meant here and relative refers to the arch thickness. Eliminating f yields functions ej(c0) which are further processed together with ultimate load factors fULS,j.

5   RAW DATA PROCESSING AND PARAMETER CALIBRATION

The criterion of the RLLS, $c_0 < c_{0,lim}$, is not acceptable for mass use since a non-linear bridge structure analysis is necessary on the part of the Guide user with every instance. In order to avoid it, a correlation is assumed between the crack depth in a non-linear analysis and the relative thrust force eccentricity in a linear analysis in the same bridge instance (at the same load level). The correlation is approximated by a quadratic function of c_0 whose coefficients are functions of the bridge parameters, specified below.

The RLLS criterion converts to $e < e_{lim}$ in the wake of the correlation.

Table functions $e_j(c_0)$ and ultimate limit loads $f_{ULS,j}$ of all representation bridge instances are processed by a single purpose programme to obtain their least square approximations

$e(c_0, l, h, d, s)$ and $f_{ULS}(l, h, d, s)$. Actually, the approximations are linear in *h, d, s* and quadratic in *l*. For given bridge structure parameters and limit crack depth $c_{0,lim}$, the ultimate limit load and limit relative eccentricity follow from these two approximations. Using the inverse functions to $e_j(f)$, the RLLS limit loads $f_{RLLS,j}$ are computed from the limit relative eccentricities. The final load ratings of the representation are $f_{CAP,j} = min(f_{RLLS,j}, \gamma \ f_{ULS,j})$ where γ is the safety factor with respect to the ULS. These are once again fitted by the least

square approximation f_{CAP} *(l,h,d,s)*. This function and the limit relative eccentricity $e_{lim}=e(c_{0,lim},l,h,d,s)$ are the results of raw data processing additionally to f_{ULS} *(l,h,d,s)*.

Two values are subject to calibration, the admissible relative crack depth in the RLLS, $c_{0,lim}$, and the safety factor γ of the ULS. Calibration is supported by a graphic display of the intermediate results. An example is shown in Fig. 4, where the values $c_{0,lim}=0.4$ and $\gamma =3.4$ are used and the semi-empiric formula results are compared to the MEXE method (Highways Agency, 1997) and the current Czech standard (Min. of Interior of the CR, 1989). On the vertical axis there are forces per 1 m wide strip of the arch. Comparable MEXE values are obtained by applying the span-rise and profile factors to the PAL values and dividing them by the lane width 3 m. Other factors of the MEXE method account for the material and condition and are not used to obtain comparable values.
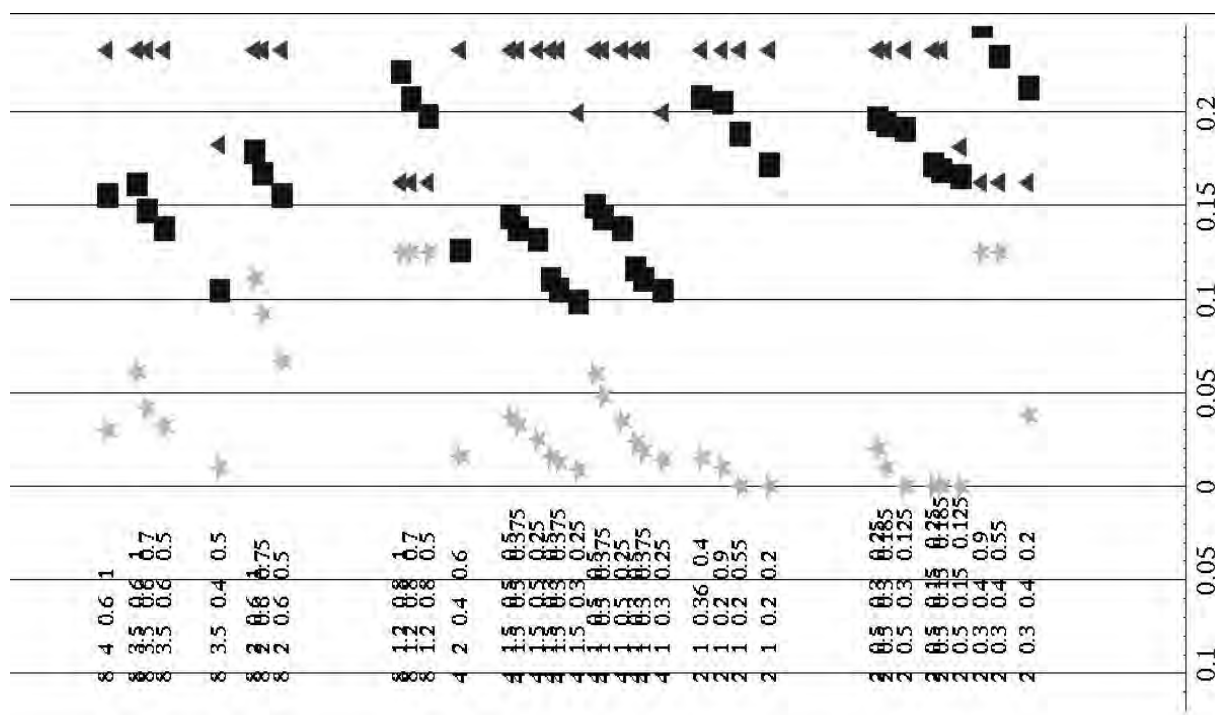

Figure 3: Load ratings of the representation [MN/m], vertically, ULS safety margin $\gamma =3.4$, limit relative crack depth $c_{0,lim}=0.4$. Blue squares – semi-empiric formula, red triangles - MEXE method, green asterisks - Czech standard. Instances of the representation are allocated on the horizontal axis by increasing parameters *l, h, d* and *s* (barrel span, rise and thickness and fill depth).

Vertical alignment of most MEXE values corresponds to the upper bound 70 t of the PAL and testifies that the MEXE method is not suitable for the country's arch bridge stock. The Czech standard values on the other hand exhibit inadequate scatter and conservatism. The semi-empiric formula offers substantial improvement. The calibration process remains open in that the representation can be extended. The current values of $c_{0,lim}$ and γ may also change in the future. In particular, $c_{0,lim}$ should be bolstered by experimental evidence. Tests on eccentric compression of masonry specimens with cyclic reversed load are being prepared which should confirm the existence of the repeated load limit state and the suitability of its criterion. Processing of the linear and non-linear representation analyses results is programmed in *Mathematica* (Wolfram Research Ltd*, 2006) including graphic output for easy calibration. The programme is available free upon request to the author. Most numerical representation solutions, however, can hardly be ported to other country conditions.

6   THE GUIDE APPLICATION

The user checks first whether the bridge parameters and condition comply with Guide applicability conditions and parameter ranges. For routine use, the load rating formula f_{CAP} (l,h,d,s) is explicitly given. The load rating is readily obtained by substitution of the actual bridge parameters. For later reference, this is termed the *direct formula method*.

There are instances of particular importance when a more precise evaluation is desirable. The Guide offers an option for those cases when f_{ULS} (l,h,d,s) is greater than f_{CAP} (l,h,d,s), that is, for the cases when the RLLS is decisive in the load rating assessment. A more elaborate structural model can produce a less conservative rating than the direct formula in these cases. The Guide provides a formula for the limit relative thrust eccentricity $e_{lim}=e(c_{0,lim},l,h,d,s)$. The user performs a standard linear analysis of the bridge structure. The analysis should be performed with an adequate structure model accounting for the interaction of the barrel, fill, roadway and spandrels, true 3D distribution of the load and structural resistance. A finite element method will almost exclusively be used. The analysis is quasi-static, considering the superposition of the dead load and a proportionally growing live load according to the respective road load standard. The maximum thrust force eccentricity within the barrel grows with the growing live load level. When the limit relative thrust eccentricity e_{lim} is reached, the RLLS limit load f_{RLLS} is achieved. It will be greater than the load rating by the direct formula in most cases. The final load rating is $min(f_{RLLS}, \gamma \ f_{ULS})$. This is termed the *numerical solution method*. Its cost is incomparable to the direct formula method and its application will be rather exceptional. It may turn out to be acceptable with skew bridges, integral spandrel action and similar spatial phenomena.

7   CONCLUSIONS

A load rating method is developed for masonry arch bridges, suitable for mass scale application. Two hierarchical procedures are proposed, linear elastic numerical analysis and semi-empiric formula. Both are based on two limit states, the ultimate load state and the repeated load limit state. The actual calibrated values of the limit crack depth and ultimate load safety factor yield load ratings better than the current Czech standard or the MEXE. The draft Guide with user instructions is entering the formal commissioning process to become official.

8   ACKNOWLEDGEMENT

REFERENCES

Adina R&D, 2004: ADINA Automatic Dynamic Incremental Nonlinear Analysis, 8.1.3 edition, Watertown, Mass., USA.
Boothby T.E., 2001: Load Rating of Masonry Arch Bridges. Proc. Inst. Civil Engineers, Bridge Engineering, 6, No 2, 79-86.
CEN ENV 1991-1, 1994: Basis of Design and Actions on Structures Part 1: Basis of Design. Eurocode 1.

Cervenka Consulting, 2007: ATENA Atena program documentation, www.cervenka.cz.

Fanning,P.J., Boothby, T.E, Roberts, B.J., 2001: Longitudinal and Transverse Effects in Masonry Arch Assessment. Construction and Building Materials, 15,51-60.

Fanning,P.J., Boothby, T.E., 2003: Experimentally-based assessment of masonry arch bridges. Proceedings of the Institution of Civil Engineers, Bridge Engineering, 156, No. 3,109-116.

Pippard, A.J.S., Ashby R.J.: An experimental study of a voussoir arch. Proc. Inst. Civil Engrs, 1938, 10,383.

Heyman, J.: The masonry arch. Ellis Harwood, Chichester, 1982.

Highways Agency, 1997: The assessment of highway bridges and structures, amendment no 2, chapter 3, Assessment masonry arch bridges by the modified MEXE method. Design manual for roads and bridges, vol 3,section 4, part 4. Her majesty's Stationery Office, London, 1997, BA 16/97.

Melbourne, C., Wang, J., Tomor, A.K., 2007: A new masonry arch bridge assessment strategy (SMART). Proc. ICE, Bridge Engineering, Vol.160, No.2, p. 81-87.

Min. of Interior of the CR, 1989: Load rating tables. Appendix 1 Guide to load rating arch bridges on motorways, roads and local roads (in Czech).

Min. of Tranport of the CR, 2000: Recommendations for design of the new and rating of the existing concrete road bridges (in Czech). TP144.

Owen, D.J.R. et all., 1998: Finite/discrete element method for assessment and repair of masonry structures. In A. Sinopoli, editor, Arch bridges, Proc. 2nd International Arch Bridge Conference. Balkema.

Rericha, P., 2000: Static and dynamic limit loads of reinforced concrete structures, CTU Reports vol.4., Czech Technical University in Prague.

Rypl, D., 2004: T3D mesh generator. Czech Technical University in Prague, Faculty of Civil Engineering, http://mech.fsv.cvut.cz/dr/t3d.html.

UIC, 1995: Recommendations for the assessment of the load carrying capacity of existing masonry and mass-concrete bridges, UIC Code 778-3r. Int. Union of Railways, 16 Rue Jean Rey - 75015 Paris.

Wolfram Research Ltd, 2006: Mathematica 5.2. Wolfram Research Ltd., 10 Blenheim Office Park, Lower Road, Long Hanborough, Oxfordshire OX29 8RY, U.K., 2006, www.wolfram.com.

Effectiveness of drainage grooves in road wearing course

M. Moravec
Ph.D. student of University Pardubice, Jan Perner Faculty of Transport, Dept. of Transport Infrastructure, Pardubice, Czech Republic

K. Pospíšil[*]
CDV – Transport Research Centre, Brno, Czech Republic
* Corresponding author: karel.pospisil@cdv.cz

ABSTRACT: Surface drainage of road pavements with both a very low longitudinal and transversal gradient is a subject for special solutions. Drainage grooves rabbeted into the road pavement wearing course are one of them. While the costs of this kind of maintenance are not inconsiderable, the effectiveness of such a solution has not yet been independently evaluated. This paper describes experiments done in the field of assessment of the drainage grooves effectiveness.

KEY WORDS: Surface drainage, drainage groove, pavement, wearing course

1 INTRODUCTION

Occasionally landscape topography or technical reasons cause very low gradient of a road's vertical alignment. This causes a problem with the surface drainage of the road pavement. This situation is solved by additional measures. Pavement surface grooving is one of these. Grooves are made using slotting cutter typically over the whole width of roadway. Usually grooves create drainage lines consisting of several parallel grooves. The drain lines are repeated several times to maintain the appropriate surface drainage of road pavement surface. Figure 1 shows a typical application of grooved drain lines on a cement concrete motorway pavement.

Figure 1: Grooved drain lines on a concrete motorway pavement surface

The depth of grooves is between 1 and 8 mm, the width typically 30 mm, and the distance between neighboring grooves is from 10 to 200 mm. Schematically, the grooves and drainage line are displayed in Figure 2. Distances between neighboring drainage lines vary greatly and depend on the specific design. An angle formed with the road axis and the direction of a drainage line is usually approximately ± 45°.
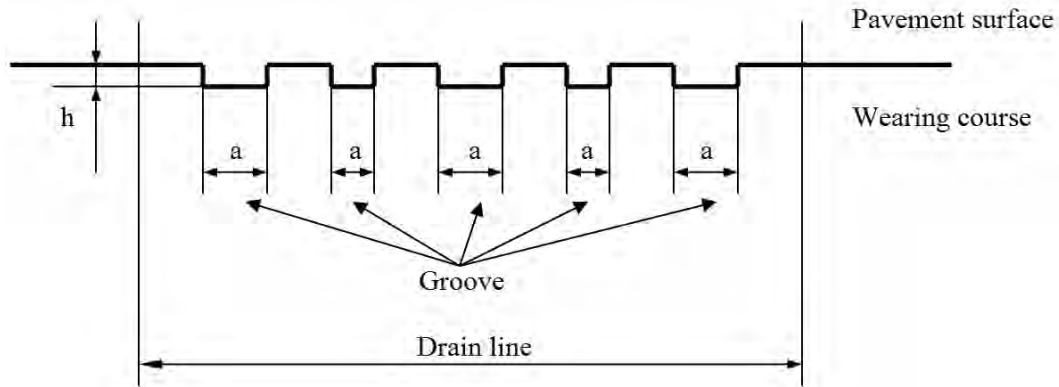

Figure 2: Schematic illustration of grooves constituting a drain line

2   THEORETICAL BACKGOUND

Companies offering grooves as an element of the surface drainage system suppose that they can facilitate a water flow in the case of a pavement surface with a gradient of close to zero. Sufficient theoretical analysis of the asset has not yet been presented. It can be taken that a pavement surface with a zero gradient has no capability to drain rainwater. An effective drainage system can permit a laminar water flow which can be attained by the appropriate dimensions of the drain pipe, gutter or groove. Laminar or turbulent water flow can be distinguished by using the critical value of the Reynolds number, which for pipes is 2,320 and for gutters 520 (Veselý, 1985).

Calculation of the Reynolds number in shown in eq. (1).

$$\mathrm{Re} = \frac{V.R}{\upsilon}, \quad (1)$$

where:

Re is   the Reynolds number,
V the water flow velocity (m.s^{-1}),
R in the case of pipes: the pipe diameter (m)
            in the case of gutters: the hydraulic radius (m), see eq. (2), and
υ is the kinematic viscosity (m².s^{-1}).

The hydraulic radius determination is shown in eq. (2).

$$R = \frac{S}{C}, \quad (2)$$

where:

R is   the hydraulic radius (m),
S the area of cross-section (m^2), and
C the length of dabbled circumference (m).

In the case of grooves with a rectangular cross-section the hydraulic radius R can be expressed using eq. (2) with the dimensions shown in Figure 2: R = a.h / (2h+a). After this modification the equation (1) obtains the form of the equation (3).

$$\mathrm{Re}_k = 580 \leq \mathrm{Re} = \frac{V.a.h}{\upsilon.(2h+a)}, \qquad (3)$$

where:

Re_k is   the critical value of Reynolds number for open gutters is 580 (Veselý, 1985),
Re, V have the same expression as in eq. (1),
v is the kinematic viscosity (m².s^{-1}); water kinetic viscosity in 20 °C is 1.01 . 10^{-6} m².s^{-1},
h the depth of groove (m), and
a the width of groove (m).

The equation (3) shows that the value of the Reynolds number can be influenced by the preference of the relation between the depth and width of the gutter. In the case of grooves there are technological limitations – the width cannot be expanded due to fluent wheel crossing and the deepening of the grooves may cause structural problems of the pavement wearing course.

Water can be taken as an incompressible liquid of constant mass density (in the case of this particular experiment) and its flow in an isolated system can be expressed by the Bernoulli equation (4) – taken from *Wikipedia*.

$$\frac{V^2}{2} + gz + \frac{p}{\rho} = const., \qquad (4)$$

where:

V is   the fluid flow velocity at a point on a streamline (m.s^{-1}),
g the acceleration due to gravity (m.s^{-2}),
z the elevation of the point above a reference plane (m),
p the pressure at the point (Pa), and
ρ the density of the fluid at all points in the fluid (kg.m^{-3}).

The Bernoulli equation (4) expresses the law of 'conservation of energy' which states that the total amount of energy in an isolated system remains constant. This means that in an isolated system the increase of flow speed causes a decrease in pressure. In the case of water in the groove, which is not crossed by any wheel, the total amount of energy can be taken as zero (no flow, no pressure, no elevation – reference plane can be placed to the groove bottom). It can be expressed in the equation (5), which is an analogy of equation (4), taking in to account *const. = 0*.

$$\frac{V^2}{2} + gz = \frac{p}{\rho} \quad \text{or} \quad \frac{\rho V^2}{2} + g\rho z = p \qquad \text{or} \qquad V = \sqrt{2.\left(\frac{p}{\rho} + gz\right)} \qquad (5)$$

Equation (5) in its last form can be modified in eq. (6) to express the current speed, which is increased by additional external pressure Δp (in this case, by a wheel crossing the groove).

$$V = \sqrt{2.\left(\frac{p + \Delta p}{\rho} + gz\right)} \qquad (6)$$

If $\underline{n}$ wheel crossings are considered, the equation (6) can be modified in form of equation (7).

$$V = \sqrt{2.\left(\frac{\sum_{i=1}^{n} p_i}{\rho} + gz\right)} \qquad (7)$$

If the wheel influence on the groove is continuous (e.g., in case of the applicable groove angle in combination with wheel width), and changing the groove gradient, an integral form of equation (7) can be formulated.

$$V_k^2 = \frac{2}{\rho}\int_0^k \frac{\partial p}{\partial x}\,dx + 2gz \qquad (8)$$

Equation (8) documents that the velocity of water flow in the $\underline{k}$ point depends on the pressure of water and the total elevation of groove. There is a statement above that the pressure in water is caused by the wheel crossings of the groove. The relationship between the pressure of water in the groove and the wheel crossings can be expressed by a functional relation (9).

$$p = f(V_w, I, p_w, \varphi, s_w, s_g, T) \qquad (9)$$

where:

V_w is the speed of wheel (m.s^{-1}),
I the intensity of traffic = number of wheels crossing the groove per time unit (e.g. Hz),
p_w the pressure in wheel/tire (Pa),
φ the angle between road axis and the groove [°],
s_w the shape characteristics of wheel/tire,
s_g the shape characteristics of groove, and
T the temperature (°C).

The functional expression (9) of pressure $\underline{p}$ basically depends on pressure of tires $\underline{p_w}$, speed of tire (vehicle) $\underline{V_w}$, the tire-tread pattern $\underline{s_w}$ and quality of groove $\underline{s_g}$. While the pressure and speed of the tire can be ascertained exactly, the influence of the tire-tread pattern and its interaction with the shape and condition of the groove is a multi-parametric system which could be studied using a stochastic-empirical approach. There are only several parameters of both "shape" characteristics $\underline{s_w}$ and $\underline{s_g}$, such as depth and width of tire-tread pattern and groove, which can be measurable directly, but there are many others which can be taken quantitatively only by their evidence. A current significant statistical survey on pressure of tires $\underline{p_w}$ and the thickness of the tire profile is submitted for publication by Moravec, 2008.

There is a special problem with the loss of water flow velocity, expressed by pressure loss in (10), according to Weisbach (e.g. in Allen & Ditsworth, 1972).

$$p_L = \xi \frac{V^2}{2\rho} \qquad \text{or} \qquad p_L = \lambda \frac{L}{4.R}.\frac{V^2}{2\rho} \qquad (10)$$

where:

p_L is the pressure loss (Pa),
ξ the loss parameter, which is: $\xi = \lambda \dfrac{L}{4.R}$,

λ the friction loss parameter,

L the length of searched section (length of groove up to a selected point) (m),

V, R   have the same expression as in eq. (1).

Unfortunately more-or-less all parameters of eq. (10) differ groove-to-groove and point of a groove to another point of the same groove, because of uneven wear, inherent dirtiness, local damage, etc.

Analysis of the above mentioned equations and their parameters show that the description of the interaction of a wheel (tire) and the grooved pavement has many uncertain parameters which can significantly influence the effectiveness of grooves, and their drainage lines, as an element of a surface pavement drainage system.

The theoretical analysis also shows that a possible evaluation of the drainage lines functionality can be expressed by a comparison of the water velocity in the case of plain and grooved pavement in dependence on vehicle speed. Therefore, the tests described in the next chapter are targeted to the direct measurement of water velocity on both plain and grooved pavement linked to passing car speed.

3   TESTS ARRANGEMENT

3.1   SELECTION OF LOCALITIES

The tests were done in two selected localities. The first one had been selected to be on a rural section of the highway I/34 between the villages Michalovice a Šmolovy, as a representative of long-term exploited treatments. Figure 3 documents the state of the drainage lines.

Figure 3: Grooved drainage lines on I/34 highway, exploited and deteriorated treatment

The left picture in Figure 3 shows a general view of the drainage lines' arrangement and the right picture in the figure documents the deterioration of the drainage lines caused by traffic loading.

The second locality of interest is a rural section of the highway I/35 between the village Hřebeč and town Moravská Třebová. This locality is representative of the recently established treatments. Figure 4 displays the status of the treatment at this locality.

Table 1 consists of the measurable parameters for both localities.

Tab. 1: Parameters of grooves and drainage lines in both of selected localities

Parameter	I/34	I/35
Groove width/depth/distance between drainage lines (mm)	30/4/1,300	30/5/1,100
Grooves in drainage line/angle in between dr. line and road axis	5 / 40°	5 / 45°
Age of treatment	10 years	20 months

Figure 4: Grooved drainage lines on the I/35 highway, recently established treatment

3.2   TEST PARAMETERS

Measurement of the water velocity was carried out using two inductive sensors. One of them was placed in the groove and the second one on the plain pavement. The distance between both sensors was determined at 1.8 m.

The transversal position of the sensors was set up at the closest position to the right wheel path. This sensor's placement minimized the pressure losses described in equation (10).

Experiments were carried out on wet pavement (after rain), and additional water needed for the tests was supplied by a tanker. The speed of vehicles was taken using a radar device and the levels of water on pavement and grooves were controlled using a plastic pattern glued on the pavement surface and the groove bottom.

The number of measured vehicles was determined employing statistical methods taking in to account the estimated dispersion of the statistical set. The number had been set at 300 vehicles in each particular measurement.

All equipment was hidden from car drivers to prevent changes to their behavior due to the tests. For the same reason the tests were arranged for just after rain, when the pavement was "naturally" wet and added water did not cause any unnatural reaction of passing drivers.

4   TEST RESULTS

4.1   TESTS ON I/34 – DETERIORATED TREATMENT

Tests on the I/34 highway, where the drainage lines were established ten years ago, were done over two summer days in both directions. Results of experiment are summarized in the graphs shown in Figure 5, and parameters which influenced the tests are shown in Table 2.

The graphs establish a relationship between velocity of drain water and velocity of passing vehicles. As described in the previous chapter, water velocities in the grooves and on plain pavement were collected.

The test results document that there is no significant impact of drainage lines usage in the observed road section. The reason for this finding can be explain by the deterioration of the grooves and their drainage lines.

Visual observation resulted in place of tests shows that deteriorated grooves in connection with local surface defects worsen the drainage functionality of plain pavement.

Tab. 2: Parameters of tests at I/34 highway

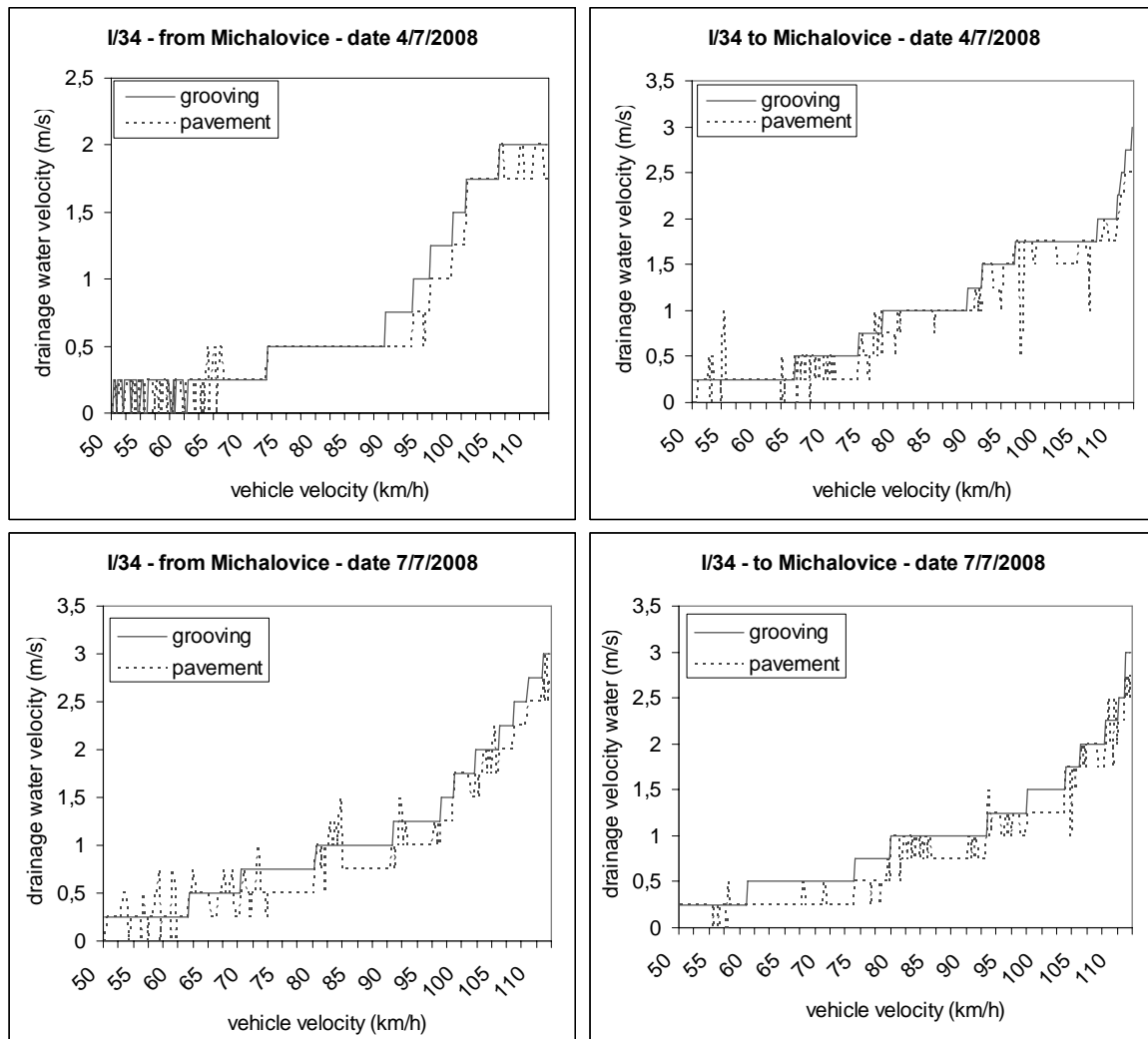|	from Michalovice		to Michalovice	
	on 4/7/2008	on 7/7/2008	on 4/7/2008	on 7/7/2008
Number of vehicles per hour	257	265	243	240
Av. vehicles velocity (km.h^{-1})	64.0	73.1	70.3	75.7
Number of measured vehicles	300	300	300	300
Longitudinal/ transversal gradient	$-$ 0.8 %/0.0 %		0.8 %/0.0 %	
Average Daily Traffic (vehicles/24 h -both directions)	7,736 (source: RSD, 2005)			

Figure 5: Relationship between drainage water velocity and vehicle velocity on I/34 highway

4.2 TESTS ON I/35 – RECENTLY ESTABLISHED TREATMENT

Tests on the I/35 highway, where the drainage lines were established twenty months ago, were done over three days in both directions. The test arrangement was the same as in the case of I/34. Results of the experiment are summarized in the graphs shown in Figure 6 and input parameters in Table 3. Analogously, as in previously described case, the graphs display a relationship between the velocities of both pavement and groove water drainage and the velocity of passing vehicles.

The test results document that there is only an inconsiderable impact of drainage lines usage in the observed road section. The difference between the velocity of water drainage on plain pavement and the velocity of water in the groove, shown in the majority of Figure 6 graphs, is not so high. The small recognizable difference can be expressed through the accuracy of the measurement method. There is an exclusion displayed in the last (sixth) graph of Figure 6.
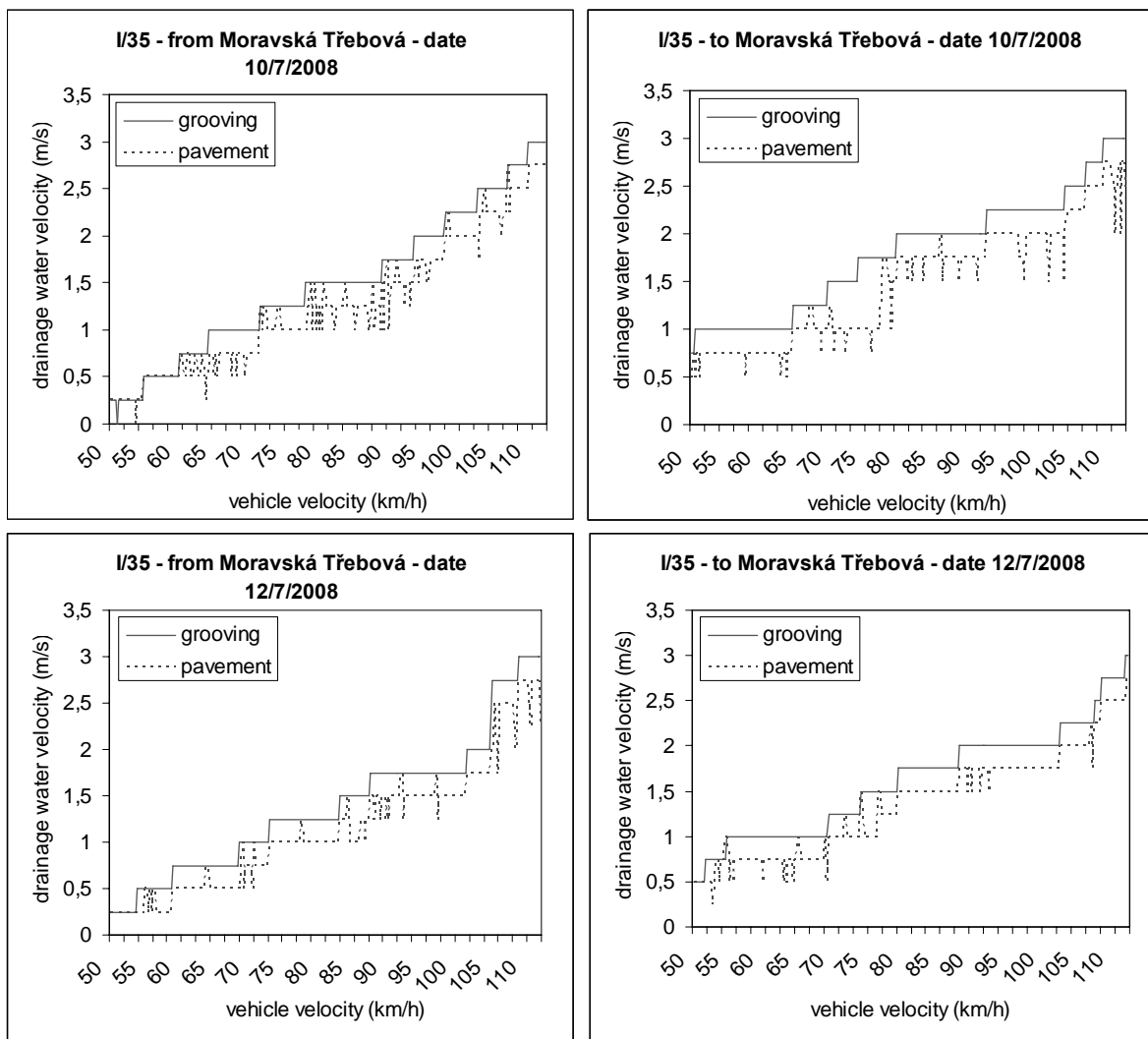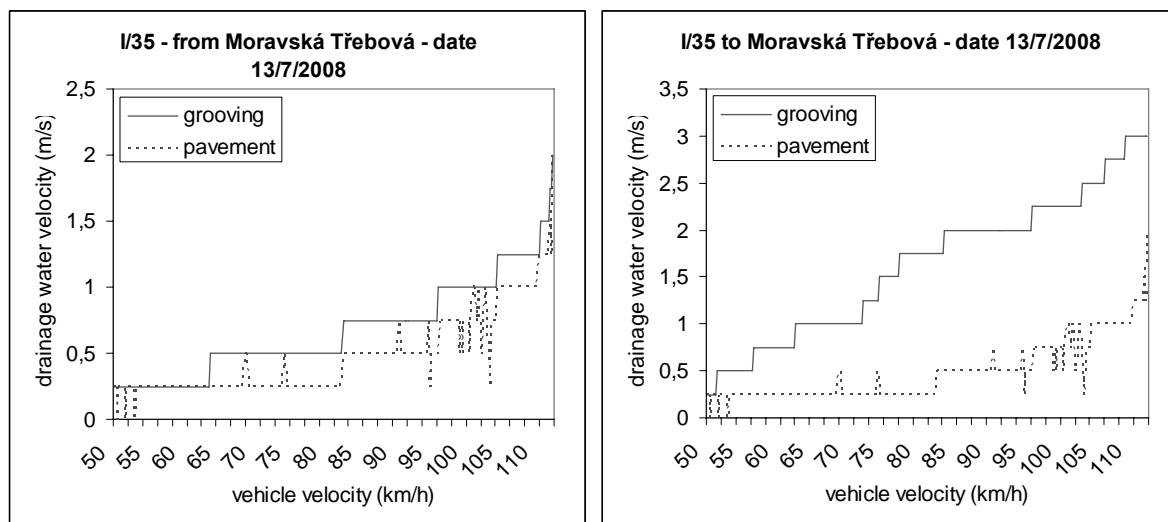
**Figure 6: Relationship between drainage water velocity
and vehicle velocity on I/35 highway**

The last graph of Figure 6 documents the relatively large difference between the velocity in the groove and the velocity measured on the plain pavement. Looking to Table 3 can give the answer: conformable with the described theoretical base, the pressure in water depends on the intensity of the traffic, see eq. (9). While the traffic intensity in all other cases is approximately 240 vehicles per hour, in the exceptional case described the traffic intensity is 375 vehicles per hour. It seems the main influence on the effectiveness of grooves as an element of the pavement surface drainage system is due to this fact.

Tab. 3: Parameters of tests at I/35 highway

	from Moravská Třebová			to Moravská Třebová		
	on 10/7	on 12/7	on 13/7	on 10/7	on 12/7	on 13/7
Number of vehicles per hour	243	205	225	217	250	375
Av. vehicles velocity (km.h^{-1})	79.7	78.0	59.3	93.2	88.9	84.7
Number of measured vehicles	300	300	300	300	300	300
Longitudinal/ transversal gradient	4.5 %/0.5 %			− 4.5 %/0.5 %		
Average Daily Traffic (vehicles/24 h -both directions)	13,297 (source: RSD, 2005)					

5   CONCLUSION

Although the optimal dimensions of grooves can help with achieving a higher value of the Reynolds number, see eq. (3), and a lower pressure loss, see eq. (10), which allows stabile laminar water flow, there are technical and operational limitations. The width of the groove is limited by the ability of the wheel to cross the groove fluently, without an excessive dynamic effect to the vehicle and the environment. The depth of the groove is restricted by the structural integrity of the pavement wearing course and the possibility of its maintenance (cleaning). Both the Reynolds number and the pressure loss, calculated using eq. (3) and (10), are changing during the groove exploitation (abrasion, dirtiness, etc.). It caused instable groove behavior within its operation period. The performed experiments reflect that drainage lines consisting of grooves are not broadly usable as a tool for the surface

drainage of pavements. Tests done on deteriorated and recently established drainage lines show very similar unconvincing findings.

It was observed that both damaged and undamaged grooves have no impact on the speed of drainage if the traffic intensity is approximately 240 vehicles per hour. At the same time it is necessary to say that a significant influence was found in the case of traffic intensity of 375 vehicles per hour, see Figure 6, last (sixth) graph, and Table 3, last column. In comparison with the Average Daily Traffic 13,297 vehicles per 24 hours in both directions, see Table 3, a measured traffic intensity of 375 per hour is achieved in the majority of the road performance time. Therefore it seems that the drainage lines consisting of the grooves are a convenient solution for these places. If we adopt this finding, the aforementioned final graph in Figure 6 documents that traffic intensity is not the only parameter of regular drainage lines functionality. In conformity with equation (9), the pressure in water flow in the groove depends on the traffic speed as well. It seems that this dependence is not directly proportional because there is no observed difference between the drainage of plain and grooved pavement up to speeds of traffic of 60 km.h^{-1}. A more verisimilar explanation of the singularly different result of one test from the additional nine tests is in the wrong functionality of sensor collecting water velocity data from the plain surface. This hypothesis is supported by the fact that velocities of water in grooves are more or less the same in all the cases shown in Figure 6, but only the velocity of water on the plain pavement in the last graph of Figure 6 significantly differs from the others.

The performed experiments do not confirm any positive influence of drainage lines consisting of grooves on the surface drainage of pavements. It can be recommended to continue with experiments aiming to the clarification of the influence of particular parameters affecting pressure, i.e., the speed of vehicles, traffic intensity, the pressure in the tire, shape characteristics of the tire and groove, temperature. This research can result in a more elaborated functional dependence than expressed in the wide and general definition of equation (9).

REFERENCES

Allen, T., Ditsworth, R. L., *1972. Fluid Mechanics,* McGraw Hill, New York.
Moravec, M., 2008. *Průzkum stavu pneumatik používaných v ČR [Survey on Tire Status Used in the Czech Republic].* 6/2008. Doprava [In Czech] (submitted).
RSD, 2005. *Sčítání dopravy v roce 2005 [Traffic Counting in the year 2005].* http://www.scitani2005.rsd.cz/html/1_pa.htm. Ředitelství silnic a dálnic ČR [Road and Motorway Administration of the Czech Republic]. [Online].
Veselý, J., 1985. *Vodohospodářské inženýrství [Water Management Engineerig].* Brno University of Technology, School of Civil Engineering [In Czech].

Airbags for motorcycles situated on the tank

M. Hönig[*], J. Kovanda, J. First
Department of Transporting Technology, Czech Technical University in Prague, Czech Republic
* Corresponding author: xhonig@.fd.cvut.cz

ABSTRACT: The aim of the study is to evaluate the tank as a potential place for motorcycle airbags. The study compiles the efforts of the CTU in Prague, HTW Dresden, as well as JAWA and DELPHI, for the improvement of the passive safety of motorcycle riders. The tank shapes are taken into consideration, as to their effects on passive safety, including their suitability or unsuitability. The possibilities of the software MADYMO as a tool for an initial blue-print of any motorcycle airbag if placed on the tank are also described.

KEY WORDS: Passive safety, crash test, airbag for motorcycle, tank deformation, tank shape, computer simulation, use of software MADYMO

1   INTRODUCTION

Since 1981 the airbag has become a standard piece of equipment for passenger cars. It has been offered by Honda for some of their motorcycles since the beginning of 2007. Since 1973, talks have been carried out about airbags becoming usual safety equipment for motorcycles (Honda, BMW) or Scooters (Yamaha) and many prototypes and attempts have been made. However, nowadays there are serious talks about the passive safety in the medium sized motorcycle category. It is sad to say that the development of the passive safety for this category is stagnant. Critics argue that the costs of these developments are not recurrent and it is obvious that there is space for development within this range when it comes to Diploma theses and doctoral works at Universities. The Czech technical university in Prague (CTU in Prague) already offers long term student exchanges and co-operates with the University of Applied Sciences in Dresden (FH) especially in connection with passive safety and biomechanics. Through the materials gathered from both Universities all their experiences concerning passive safety of motorcycles into were summarize into a Ph.D. project. The principle purposes of this doctoral work were defined as follows:

1. reducing the injuries of two-wheeler drivers
2. measurable improvements in the medium sized motorcycle category
3. optimizing the kinetics of the legs and spine the motorbike driver in accident situations
4. conceiving the motorcycle airbags for the protection of the driver's upper body
5. optimizing the airbags by use of virtual and experimental simulations for the minimization of the peak load of motorbike driver

To support these assumptions three motorcycle crash tests into the side of a car were carried out. Statistics show that it is one of the most frequent types of accident. In all of the crash tests the motorbikes were occupied by one passenger in a standard sitting position. The motorcycles differed in the type of sitting position. The following types are concerned: traveling and two extreme (super sport and chopper).   The crash tests speed was approximately 60 km per hour.

It was clear from the beginning that this work cannot produce results for an optimal solution without the support of a motorcycle producer and a development company for passive safety. Thus since last year the CTU in Prague has co-operated with the local motorcycle producer JAWA and HTW in Dresden, which in turn already co-operates with DELPHI in Berlin, for diploma theses in common. Owing to these possibilities we were able to unify and optimize crucial ideas in our developments at CTU in Prague, especially with the support of these two co-operating partners from a practical point of view. It is also important to note that it was possible to use just some parts of the test results of different institutions (i.e., DEKRA), although without any factual means for our research. Medium sized motorcycles are frequently tested for passive safety, although because of the cost and complicity the result are never implemented in real production

In the year 2003 motorcycle research on accidents began at CTU in Prague with crash-tests and accident simulations for medium sized motorcycles. The Czech technical university had already accomplished many crash-tests. The most frequent kind of accident with fatal consequences for the motorbike driver is through the impact of the motorcycle driver's head to the side or tail of a passenger car. The accident research progressed with the support of investigations through mathematical simulations, as well as real crash tests in development airbags in accident configurations, according to the ISO 13232 (front: 114. side: 413 and back: 711). For the real crash tests we used the ÚSMD dummy, and made some further necessary improvements so that it could be similar to that of a motorbike driver. As for the mathematical simulations, we used the Hybrid III 50th percentile male.

2   THE INFLUENCE OF THE MOTORCYCLE'S TANK ON INJURY

Nowadays the motorcycle's tank design has a great influence on the overall design of motorcycle. This has given rise to all sorts of designs and shapes, which in no cases fuse with the passive safety viewpoint. Missing legislations for the protection of motorcyclists by passive safety components make different concepts possible, which do not take into account a motorcyclist's passive safety. In the Transportation Faculty of Transportation sciences a great amount of experimental tests were carried out in which motorcycles of different classification, size, weight, and type of sitting were tested. During the crash tests it was observed relatively often that small deformations were found on the tank. These deformations were caused by the impact of the motorcyclist's pelvic area to the tank.

During the last crash tests in "Faculty of Transportation" sciences, large deformations on the tank in almost all of the performed experiments were discovered. An anthropometric device used for these crash tests has not the appropriate biomechanical properties – biofidelity - in pelvic area. This fact can influence the total deformation of tank. The relative deformation of different types of tanks is comparable. Although this area doesn't cover problems with biomechanical criterions and the standards of passive safety, this deformation in previous crash tests images were documented and were partially assessed. Impacts with the pelvic area, which are the genital and the upper part of the lower limb area of the pelvis, are not taken into account, neither on default anthropomorphic dummies nor in mathematical modules. This is why it is possible to find great potential in university research in this area. While considering the use of airbags it is primordial to talk about the impact of the pelvic area to the motorcycle's tank, since it is expected that the upper body of the motorcyclist is locked by the airbag, but also that there will be an increase of acceleration in the pelvic part of the motorcyclist.
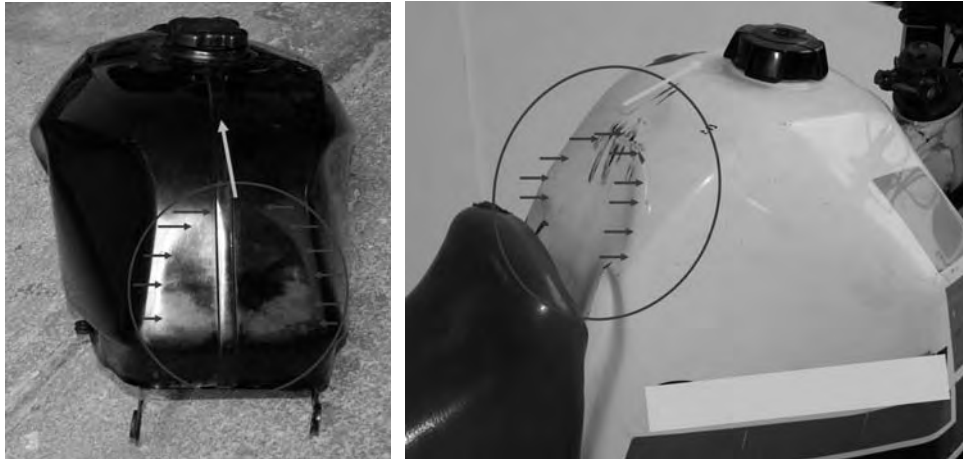
Figure 1a, 1b: Motorcycle tanks after crash tests [3]

The black tank on the left and the white tank on the right are good examples of suitable and unsuitable designs of motorcycle tanks. On the black tank due to the style we can see that it has got a huge deformation by applying a relatively tiny force. On the other hand the deformation on the white tank shows evidence of a great impact and also of a huge damage to the bottom part of dummy's body in the pelvic area.

**Figure 2a, 2b: Riding setting of motorcyclist and tank
in relative location on motorcycle JAWA 650 [3]**

However, in general we can conclude that the airbag for motorbike research mentioned in section 1 in CTU in Prague and HTW Dresden is aimed at more factors. These factors are the sitting position, the closing speed, and the shape of a tank. The key aspects are the position of the occupant and the tank. If the airbag is impacted during the collision by the occupant directly, then the airbag efficiency is sufficient. The problem is the position of the occupant and the airbag in the indirect collision, although the task of this research is the comparison of the crash tests with different sitting positions and tank shapes with use of one dummy. On the base of this research a mathematical model of an airbag on the tank in the shape of a letter T is made.

3   STANDARD POSITION SETTING OF THE MOTORCYCLIST IN RELATION WITH THE MOTORCYCLE TANK

The motorcyclist is sitting on the saddle of a motorcycle in the front area. He almost encircles the tank of motorcycle with his legs. The muscles of the pelvic floor are in direct contact with

the leather foam lug of the front end of the saddle. Femurs of the dummy are in direct contact with the motorcycle's tank. The motorcyclist grips the steering handlebar with both hands. The rest of the arm is free and close to the body and to the motorcycle tank.

4   ANALYSIS OF THE MOTORCYCLE'S TANK DEFORMATIONS

We can see a few areas of deformation on the tank after the crash. We could separate these deformations into two parts, the deformations caused by upper part of motorcyclist's femur (area A, marked blue in the illustration), and the deformations caused by motorcyclist's body caused by the pelvic part and by upper part of motorcyclist's femur near coxa (area B, C, D, marked red in the illustration). The green arrows demonstrate the direction of the motorcyclist's movement during the crash.
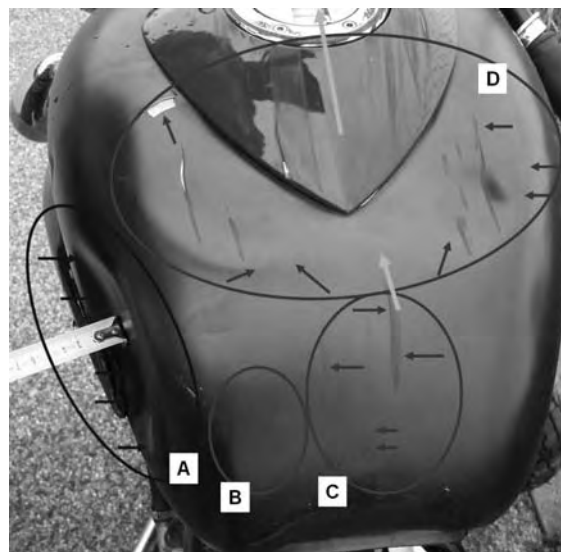
Figure 3: Deformation area on motorcycle JAWA 650 [3]

Deformation in area A was caused by the impact of the upper part of the femur with the motorcycle's tank. The depth of this deformation is 1.7 cm. (Kramer, 2006) This gives evidence of the magnitude of the impact. It is possible to make the assumption that this impact caused trauma in the coxal or femoral area or lower part of the abdomen of a great magnitude. Even if the femur and coxa were able to transfer sizable power, the impact guided in a different angle greater than 90° to the femur could have worse results. This means that the magnitude of the force is so great that it is responsible for the dislocation of the coxa. As a simple statement of reason of this premise, we could say that for humans the skeleton is more naturally inclined to take the impulsion of force in the vertical plane, because it is built for walking, running, jumping etc., as compared to forces coming from horizontal directions. Also, it is necessary to note that in fact the probable causes of this deformation trauma are influenced by the viscosity in the bottom part of the body.

Deformations in area B are visible only in illustrations 3 and 4a. It indicates small strokes of the upper part of femur between the primary and secondary impact. It is rather probable some overlapping of the left leg under the motorcycle has, as a consequence, an actual deformation of the foot and a fracture of the ankle. From a biomechanics point of view the deformation in the area B is not a direct cause of any trauma.

In area C we can see deformations and scratches caused by the motorcyclist's motion on the motorcycle during the front impact in the axis x. This quite tiny deformation was

caused by the sliding of the pelvis onto the tank. In the case of a human or more exact model of motorcyclist we can speak about the impact of the os ischii and the os pubis and the impact of the musculi perieni. The size of this deformation bears testimony to the suitable design and shape from a passive safety point of view. Although the deformation in this area is not so significant, it proves that in the case of an accident with other motorcycles with different types and shapes of tanks, this deformation could have great significance on the rise of traumas in the pelvic area.

We can assess area D, which is a great deformation zone in the area of the tank's upper surface, as a great impact where the motorcyclist's lower part of abdomen and pelvis sits on the tank. The deformation is marked out by the described ellipse 250 mm and 150 mm and a depth of almost 17 mm and is a testimony to the massive impact. In the case of a human or more exact model of a motorcyclist we can speak about an impact of the lower abdomen (muscles of lower abdomen), os ischii and os pubis and an impact of the musculi perieni.
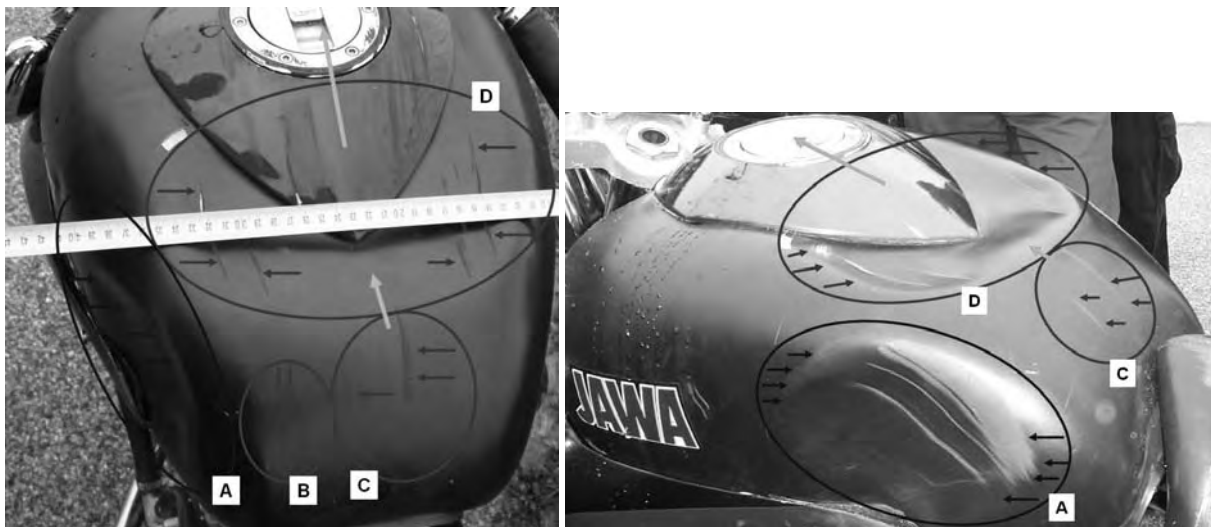

Figure 4a, 4b: Deformation area on motorcycle JAWA 650 – another view [3]

5 INTERPRETATION OF THE DEFORMATION ON THE TANK OF THE MOTORCYCLE PROTOTYPE JAWA 650

To separate the deformations and their sizes it is necessary to point out that it isn't possible to determine whether this whole deformation has arisen only during the primary impact or only during the secondary impact. When talking about the impact of the motorcycle to the lying motorcyclist or the direct pinning of the motorcyclist considering the projection. It's very likely that the deformation given arose during the primary impact and has been only partly deepened during the secondary impact. Reading the memory of the high speed camera and the data from the sensors we can assume that during the secondary impact no further tank deformations occurred, but we cannot exclude the contact possibility completely.

The implication of these deformations has effects on human trauma (in our case trauma of motorcyclist) each time after an accident. From the passive safety point of view we can say that there are critical deformations in area A and D. We can consider deformations B and C as almost insignificant, although deformation C holds a great potential for research.
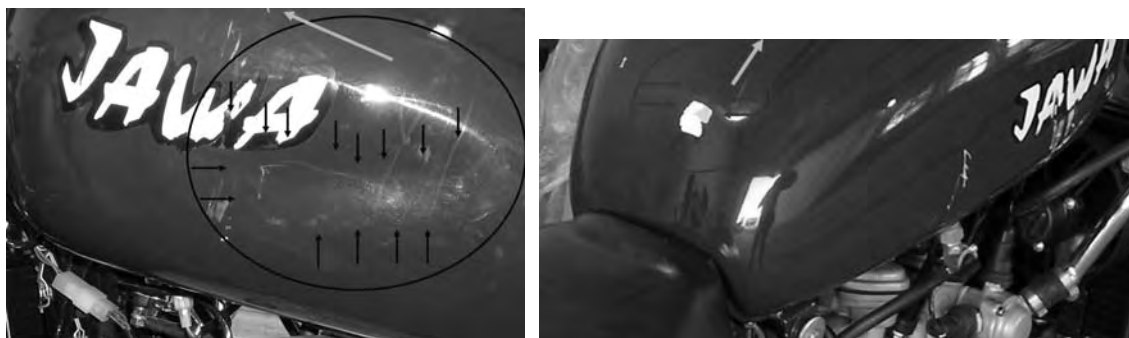
Figure 5a, 5b: Deformation area on motorcycle JAWA 650 Classic [3]

Between the motorcycle's tank deformation of Jawa 650 Classic and Jawa 650 (Bison) it is possible to see a huge difference in deformations after the crash test under the same conditions, speed and with the same dummy. This means that they are almost the identical tanks (Bison has in addition plastic cover under the tank cover), but with absolutely different deformations. It is possible to explain this difference by the motorcyclist's sitting position, because the motorcycle Jawa 650 (Bison) – as the prototype for passive safety testing, was set up in the position of steering handlebar and crampons as a motorcycle of the Super Sport type. The common series of the Jawa 650 Classic model has succeeded completely without any trauma during the crash testing of tank. We would like to express our appreciation to the Jawa company for supporting our research and for altering their designs so as to maximize passive safety on their motorcycles.

In general we can conclude that these assumptions were made after a subjective evaluation of the trajectory of the passenger, recorded by high speed camera, the size of deformation of tank, and with objective data from the accelerator in the chest area. On the basis of this subjective assumption the following shapes of tank were chosen as examples of subjectively potential suitable and unsuitable motorbike tank shapes.
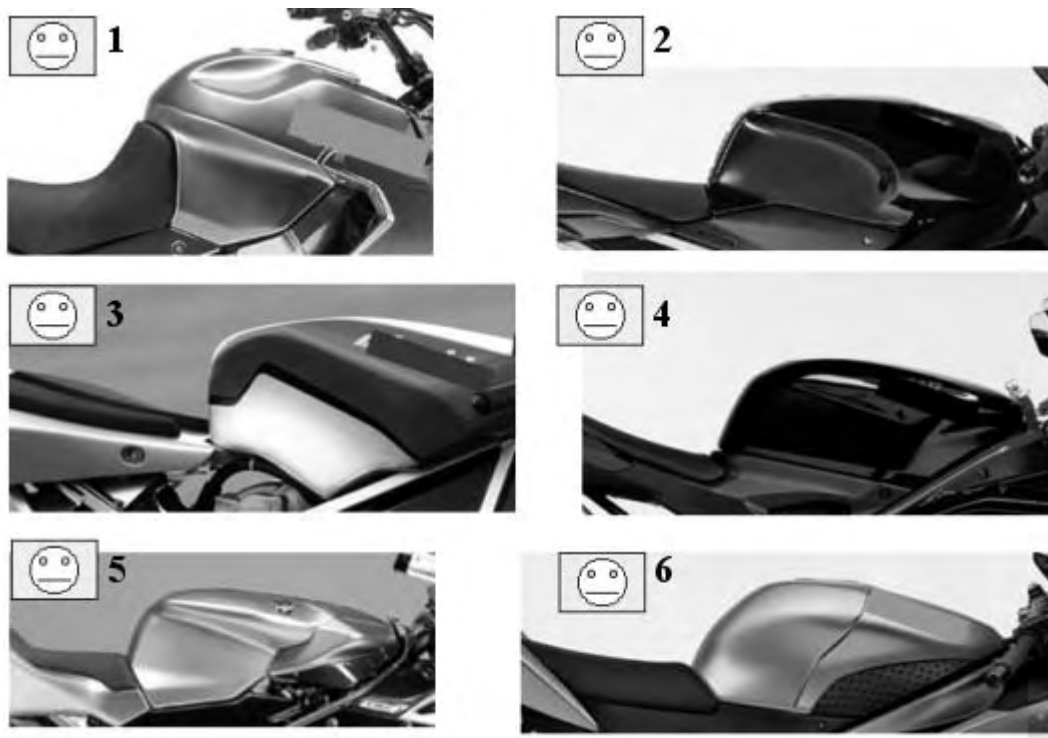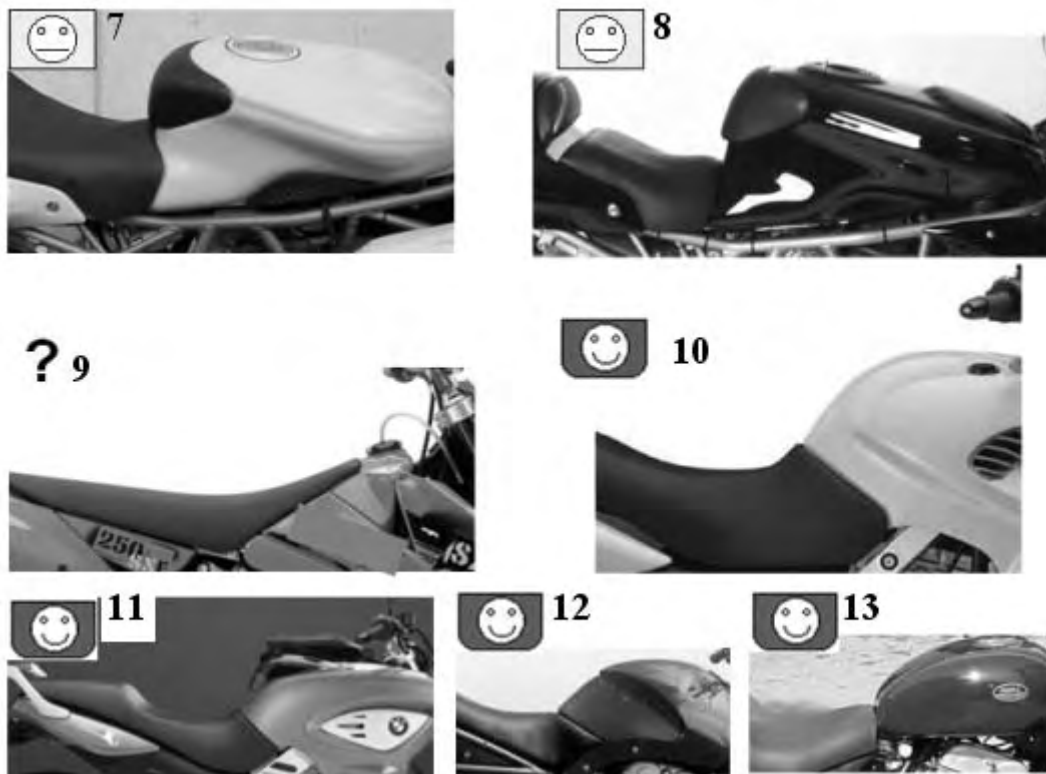
Figure 6: Some shapes of motorcycles tanks [8]

On the previous pictures different types of tanks from different types of motorcycle are shown. Each picture is assigned a smiley that represents the possible injury risk of various motorcycle tanks. It is comprehensible that it is only a subjective opinion at the moment and that it would be necessary to evaluate them using a significant number of crash tests and computer simulations. In spite of this, it is possible to decide from the naked eye, whether the set concept fuses with the unwritten rules of passive safety.

Tank No. 1: The shape indicates the intention of the constructor to project the driver over the contingent collision partner, but the ergonomic embrasure spaces contradict this initial intention.

Tanks No. 2, 4, 5 & 6: None of the shapes, nor the angles that the tanks make with the driver's seat nor the ergonomic embrasures of these tanks correspond even remotely to any passive safety point.

Tank No. 3: This shape is the worst of them all as it will prevent the driver's projection from the motorbike causing considerable damage in the pelvic area.

Tank No. 7: This shape has neither any direct influence in injuring the driver nor does it have any influence in slowing the driver's projection, but instead the driver is projected directly onto the steering handlebars.

Tank No. 8, 9, 10, 11: These shapes influence the driver's projection trajectory and are probably not the cause of any serious injuries to the driver.

6   INFLUENCE OF TANK ON PASSIVE SAFETY OF MOTORCYCLE

From an evaluating point of view it is possible to claim that it should be at most suitable to open a discussion about giving rise to a new criterion in motorcyclist's coxa area trauma during the impact with the motorcycle tank. The eventual criterion should specially consist

in the integration of different methods of research and obtaining necessary data, whether it be from medicine, passive safety, biomechanics or from the development of possible motorcycle's airbag and its application. It is essential to conduct further research connected with the impact of the pelvic area and tanks, without which the implementation of airbags on motorcycles would be completely redundant.

7   IMPLEMENTATION OF THE AIRBAG ON THE MOTORCYCLE TANK

The function of the common car airbag as part of the passive safety support system could not be converted directly for classical or large motorcycles, because the motorcycle driver does not have a definite sitting position, just as it is in the case of the passenger in the car. In addition for the motorcycle airbag, the influence of the seating position, as well as the motion path, must be considered during frontal collisions. CTU in Prague, in cooperation with HTW Dresden, has concerned themselves with the deepening of vehicle safety in the department of vehicle technology since 2004, including the sitting position, tank shape (as mentioned above) and the seat kinematics of the motorcycle passenger (Kramer, 2006). The driver position could be divided into 12 main groups of motorcycles and could be divided further into static or dynamic driving positions (traveling straight ahead, driving along curves). Static driver position means traveling straight ahead without pre and back bends. Dynamic position means driving along curves, as well as traveling straight ahead with pre and back bend. The driver position plays an extremely important role for the use of airbags on the motorcycle tank.

  Unfavorable sitting positions of the driver, which prevents an optimal use of the airbags, must also be considered with the organization and tuning of the airbags to an extent where at least endangering of the driver must be excluded! Some years ago airbags for motorbike driver began with the commercial offer of the "airbag jacket", an airbag, which was integrated in a jacket or waistcoat of the motorbike driver. A motorcycle airbag should with 90 litres of gas volume protect from the moving of the chest and neck range. The release was made by activation-line and offered rather as a protection against secondary collision with the roadway. The first series use of the airbags on the motorcycle was done by Honda in the year 2007. The motorcycle Honda Gold Wing uses sensor systems of the collision and is activated by the same acceleration sensors which are placed on the front fork. In the cockpit of the motorcycle instead of a tank an airbag generator is placed, similar to the passenger car. During the collision phase the driver is caught by the motorcycle airbag, which is embodied and supported by special straps on the vehicle's frame. This airbag has to protect against structures of the collision partner or to reduce the contact speed in a secondary crash. The conversion of this airbags for large motorcycles with relatively defined seating position is possible. But the question is how can this principle be transferred to middle class motorcycles?

Figure 7: Motorbike Jawa 650 Classic [2]

The greatest portion of the work to be done is that which is connected with experimental simulations, which were accomplished at CTU (First & Kovanda & Lenk, 2004). The results of the experimental simulations made virtual simulations possible and obtained data were also used for validation.

Figure 8a, 8b: Experimental simulation in impact configuration 413 according to ISO 13232 [2]

For validating accelerations in the head and in the chest dummies were used and the tensions and deformations in the frame of the motorcycle were monitored. The film from the real collision was also used for the evaluation of the flight path of the motorbike driver for simulation purposes. The virtual simulation of the passenger car/motorcycle collision depends not only on the experimental data, but also on the particular technical data of the passenger car and the motorcycle. We first simulated using the computational configurations without safety precautions and without an airbag in the collision types 115, 413, 711 according to ISO 13 232 for Car/Motorbike accidents.
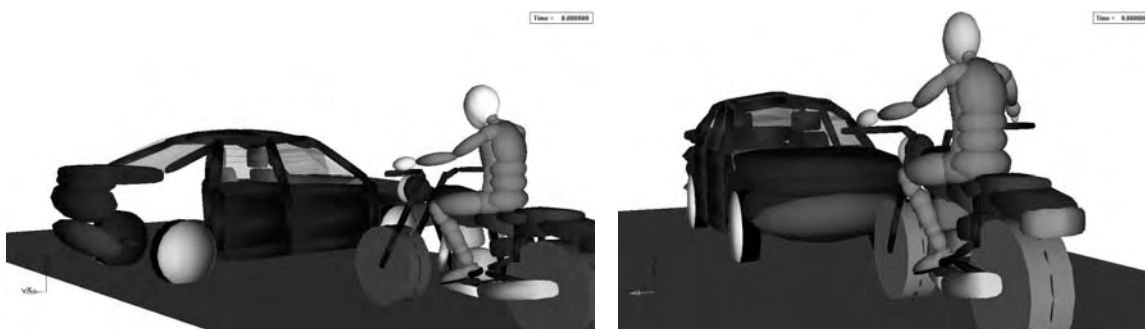

**Figure 9a, 9b: Computer simulation without airbag
in impact configuration 115 and 413 according to ISO 13232**

The next computer simulation was accomplished with a standard passenger car front seat passenger airbag of 150 litres in volume. Furthermore possible deformation structures were optimized like the front fork and further measures for improving the passive safety (e.g. employment of a Knee airbag) were tested and through this the most suitable one was selected. In the revised virtual simulations we discovered that the 115 litres full volume T-formed airbag was the most effective passive safety measure possible. This airbag was also tested in the out of position situations. It's special form and size clearly made it possible to have more favorable results than the original (front seat passenger airbag).
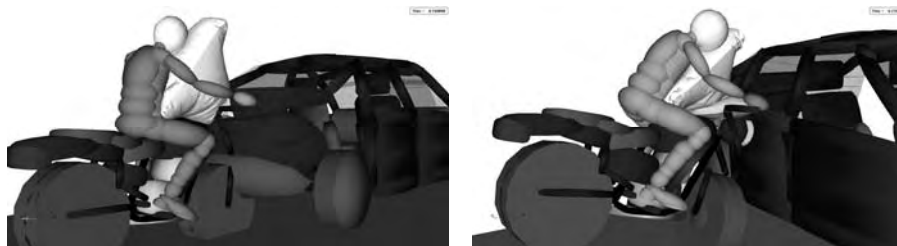
Figure 10a, 10b: Computational simulation with airbag (2.Generation), deformation structure, Knee airbag in impact configuration 711 and 413 according to ISO 13232

The improved results refer to the values of HIC, T3MS, FFC, after the data acquisition, comparison and validation by virtual and experimental simulations.

8 ACKNOWLEDGMENT

9 SUMMARY

By employing the experimental and virtual simulations for the gradual optimization of the construction and development of a special motorcycle airbag with appropriate structural changes to the motorcycle, clearly improved results in decreasing of injury sequences for the motorbike driver with continuous accident weight were confirmed. This particularly applies to it's use with motorcycles of the middle class, where substantially even more different driver positions are possible than with the heavy route machine of Honda "Gold Wing", which exhibits the only series-solution of this support mechanism for motorcycles at present.

REFERENCES

[1] Berg & Rücker, 2004. *Prüfverfahren für die passive Sicherhiet motorisierter Zweiräder (Testing method for the passive safety of motorized two-wheelers).* Study, Stuttgart.

[2] First & Kovanda & Lenk, 11/2004. *Kolize motocykl – automobil (Motorcycle-car collision),* Technical report, VYZ616.003/04, Prague, FD CTU.

[3] First & Kovanda & Šotola, 12/2007. *Kolize motocykl – automobil (Motorcycle-car collision),* Technical report, VYZ616.005/07, Prague, FD CTU.

[4] Kovanda & Šatochin, 2000. *Pasivní bezpečnost vozidel (Vehicles pasive safety).* University mimeographed, Prague, CTU.

[5] Kramer, 3/2006. *Passive Sicherheit von Kraftfahrzeugen (Passive safety of motor vehicles), University book,* Dresden.

[6] 2005-6, *Seminární práce na HTW Drážďany z předmětu odborné znalecké vědy, Vorträge Sachverständigenwesen an der HTW Dresden, (Lectures expertises on the HTW Dresden).*

[7] *Výkresové materiály firmy Jawa a.s. (Technical drawing of motorcycle company JAWA),* [CD-ROM].

[8] www.motocykl-online.cz

Instructions to the autors

1 GENERAL GUIDELINES

Papers based on accepted abstracts and prepared in accordance to these guidelines are to be submitted through the journal's web site www.transportsciences.org.

All papers, using Microsoft Word2000 (or newer) are **limited to a size of at least 4 and no more than 8 single-spaced pages** on A4 paper size (297 mm X 210 mm), including figures, tables, and references and should have an **even number of pages**. The paper's top, bottom, right and left margins must be 2.5 cm. No headers, footers and page numbers should be inserted.

2 TITLE, AUTHORS, AFFILIATIONS

The title of the paper must be in title letters, Times New Roman, font size 16, and aligned left. Use more than one line if necessary, but always use single-line spacing (without blank lines).

Then, after one blank line, aligned left, type the First Author's name (first the initial of the first name, then the last name). If any of the co-authors have the same affiliation as the first author, add his/her name after an & (or a comma if more names follow). In the following line type the institution details (Name of the institution, City, State/Province, Country and e-mail address of a corresponding author). If there are authors linked to other institutions, after a blank line, repeat this procedure.

The authors name must be in Times New Roman, regular, and font size 12. The institution details must be in Times New Roman, *italic*, and font size 10.

3 ABSTRACT

The abstract should start after leaving eight blank lines. Type the text of the abstract in one paragraph, after a space behind the word abstract and colon, with a maximum of 250 words in Times New Roman, regular, font size 12, single-spaced, and justified. After leaving one blank line, type KEY WORDS: (capital letters, Times New Roman, font size 12), followed by a maximum of five (5) key words separated by commas. Only the first letter of the first key word should be capitalized.

4 THE TEXT

The main body of the paper follows the key words, after two blank lines (i.e., two blank lines between the first heading and the key words). The body text should be typed in Times New Roman, font size 12 and justified. The first line of the paragraphs should be indented 5 mm except the paragraphs that follow heading or subheading (i.e., the first line of the paragraphs that follow heading or subheading should not be indented). Never use bold and never underline any body text.

4.1 HEADINGS AND SUBHEADINGS

The headings are in capital letters, Times New Roman, font size 12. Subheadings are in title letters Times New Roman, font size 12. The headings and subheadings must be aligned left and should not be indented.

Leave two blank lines before and one after the heading. There should be one (1) blank line before and after the subheadings. All headings and subheadings must be numbered.

If a heading or subheading falls at the bottom of a page it should be transferred to the top of the next page.

4.2 FIGURES AND TABLES

Figures, line drawings, photographs, tables should be placed in the appropriate location, aligned centre, and positioned close to the citation in the document. They should have a caption, Times New Roman font size 12, with a colon dividing the figure number and the title (Figure 1: Material properties) and should be numbered consecutively, e.g. Figure 1, Figure 2, Table 1, and Table 2.

4.3 REFERENCES

At the end of the paper, list all references with the last name of the first author in alphabetical order, underneath the heading REFERENCES, as in the example. The title of the referred publication should be in italic while the rest of the reference description should be in regular letters. References should be typed in Times New Roman font size 12. citation standard ISO 690.

More details can be found at **www.transportsciences.org**.

CONTENTS